HHS Public Access

Author manuscript

Cell Rep. Author manuscript; available in PMC 2023 October 23.

Published in final edited form as:

Cell Rep. 2023 April 25; 42(4): 112287. doi:10.1016/j.celrep.2023.112287.

Thalamic regulation of a visual critical period and motor behavior

John Hageter[1,3], **Jacob Starkey**[1,3], **Eric J. Horstick**[1,2,4,*]

[1]Department of Biology, West Virginia University, Morgantown, WV 26506, USA

[2]Department of Neuroscience, West Virginia University, Morgantown, WV 26506, USA

[3]These authors contributed equally

[4]Lead contact

SUMMARY

During the visual critical period (CP), sensory experience refines the structure and function of visual circuits. The basis of this plasticity was long thought to be limited to cortical circuits, but recently described thalamic plasticity challenges this dogma and demonstrates greater complexity underlying visual plasticity. Yet how visual experience modulates thalamic neurons or how the thalamus modulates CP timing is incompletely understood. Using a larval zebrafish, thalamus-centric ocular dominance model, we show functional changes in the thalamus and a role of inhibitory signaling to establish CP timing using a combination of functional imaging, optogenetics, and pharmacology. Hemisphere-specific changes in genetically defined thalamic neurons correlate with changes in visuomotor behavior, establishing a role of thalamic plasticity in modulating motor performance. Our work demonstrates that visual plasticity is broadly conserved and that visual experience leads to neuron-level functional changes in the thalamus that require inhibitory signaling to establish critical period timing.

In brief

Critical periods are developmental windows of heightened plasticity when sensory experience impacts brain function. Hageter et al. identify a zebrafish visual critical period, where visual experience produces neuronal and behavioral performance changes, dependent on inhibitory signaling. This work provides a model for neuron-level study of sensory-dependent plasticity.

Graphical abstract

*Correspondence: eric.horstick@mail.wvu.edu.

AUTHOR CONTRIBUTIONS

E.J.H., J.H., and J.S. conceived the project and wrote the manuscript. J.H. and J.S. performed experiments. All authors approved the submitted version.

DECLARATION OF INTERESTS

The authors declare no competing interests.

SUPPLEMENTAL INFORMATION

Supplemental information can be found online at https://doi.org/10.1016/j.celrep.2023.112287.

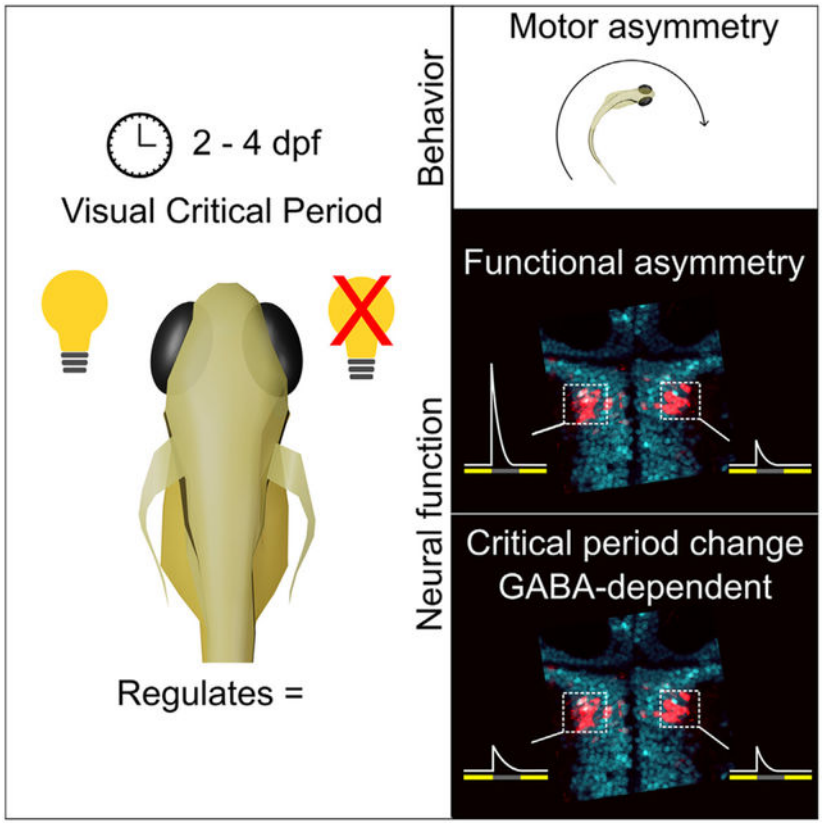

INTRODUCTION

Early life experience is instrumental in refining brain structure and function, and discrete developmental windows known as critical periods (CPs) have a prominent role in sensory-dependent plasticity. Furthermore, disruptions of sensory input or plasticity regulation can lead to impaired sensory processing and are associated with severe neurological diseases.[1–3] Ocular dominance plasticity (ODP) is a classic readout used to study visual experience-dependent plasticity.[4,5] During ODP, animals undergo monocular deprivation to produce an asymmetric visual experience, which drives structural and functional changes in visual processing centers.[3] Extensive work using ODP has revealed robust structural and functional changes in binocular connectivity, synaptic scaling, and structural changes that occur between hemispheres.[6–10] ODP experiments have been performed on diverse mammalian systems, demonstrating visual plasticity across diurnal, nocturnal, and crepuscular species with varying visual acuities and circuit structures.[4,11–14] These diverse mammalian models have provided in-depth insight into the sensory-dependent changes in the primary visual cortex, illuminating distinct mechanisms incorporating excitatory and inhibitory circuits.[15–19] Conversely, subcortical regions have received significantly less attention, but it is now known that thalamic neurons exhibit ODP in mammals.[20–23] Interestingly, the mechanisms driving subcortical ODP show distinct properties compared with visual cortex ODP, demonstrating independent mechanisms.[20–23] Subcortical contributions to sensory-driven plasticity add new layers of complexity to CP regulation and visual plasticity, but

how subcortical neurons are modulated by early visual experience remains incompletely understood. For example, functional characterization of thalamic ODP is largely dependent on recordings from thalamic projections in layer 1 of the visual cortex or organotypic slices.[21–23] Elucidating neuron-level thalamic sensory-driven changes is challenging because *in vivo* analysis in deep brain regions is technically challenging, and significant cortico-thalamic feedback signaling obscures resolving thalamic-specific changes. Moreover, GABAergic signaling is well established to regulate CP onset,[24] but thalamic contributions to CP timing are unknown.

Here we developed a model for visual CP plasticity in larval zebrafish that mirrors crucial features of mammalian ODP. Because zebrafish do not possess a cortex, the mechanisms driving subcortical plasticity can be studied independent of cortical feedback or without additional manipulations to remove feedback, providing a robust thalamic-centric ODP model. Asymmetric visual experience during a developmentally restricted time period leads to sustained neurophysiological and visuomotor change. In single animals, we show how asymmetric visual experience imposes specific visuomotor response types, which correspond to asymmetric response strengths and numbers of a genetically defined subset of thalamic neurons. Similar to well-established mammalian models,[10,24] the timing of the zebrafish CP depends on GABAergic signaling. Our work suggests that ODP is more broadly conserved in vertebrates. Our zebrafish model recapitulates key elements associated with ODP and reveals neuron-level changes in the thalamus that instruct plasticity and behavioral performance.

RESULTS

A visual CP modulates the performance of a visuomotor asymmetry

Our previous work demonstrated that larvae zebrafish exhibit a persistent motor asymmetry following loss of environmental illumination.[25–27] Following loss of global visual input, an individual will preferentially utilize leftward or rightward turns (Figure S1A). Turn bias is maintained over hours and multiple days.[26] This stereotactic behavior is consistent with search behavior patterns observed across numerous species.[28–30] In wild-type zebrafish, left- and right-turning types are observed in equal proportions.[26,27] Moreover, turn direction preference is also not heritable, implying that stochastic molecular or environmental cues determine an individual's turning type.[26,27] However, we previously were unable to identify a developmental "switch" instructing an individual to adopt a left or right turn bias preference. Therefore, we hypothesized that asymmetric photic experience could modulate the direction of turn bias behavior. To answer this question, we temporally restricted visual input to a single eye, recapitulating the ODP assay.[3] Because zebrafish vision is largely monocular,[31] we controlled visual experience by embedding larvae in low-melting-temperature agar and positioning individuals so that either a single eye or both eyes were directed to a light source; we call this prep the "CP assay" (Figure 1A). Larval zebrafish are well suited to this style of visual control because they acquire nutrients from a yolk and exchange oxygen and necessary ions by diffusion.[32,33] The CP assay also generated a robust visual asymmetry despite the transparency of larval zebrafish, likely because of the heavily

pigmented retinal epithelium. Alignment of the eyes in the CP assay blocks approximately 58% of visible light, yielding an asymmetric visual experience (Figures S1B and S1C).

To determine whether asymmetric visual experience would dictate turn bias direction, we prepared individuals in the CP assay for an approximately 48-h window, from 2–4 days post fertilization (dpf). This interval was selected because 4 dpf is the earliest when turn bias is observed[27] and coincides with retinal innervation of zebrafish visual centers.[34,35] We averaged responses over four paired light-ON and -OFF recording intervals to measure turn bias and used a bias ratio (BR)[27] to quantify the proportion of same-direction turning (Figure S2A). Turn bias behavior was maintained following embedding of larvae in the CP assay (Figures 1C, 1D, and S2B). However, asymmetric visual experience during this developmental period was capable of imposing a turn bias direction (1-way ANOVA, $F(2,146) = 14.43$, $p < 0.0001$) contralateral to the light-facing eye, whereas upright embedded larvae displayed equal proportions of left- and right-biased individuals (Figures 1E–1H). No population-level shifts in motor asymmetry direction were observed during baseline illumination, implicating a specific effect on search motor patterns (1-way ANOVA, $F(2,146) = 1.58$, $p = 0.21$) (Figure S2C).

Three key hallmarks define CP plasticity: changes are sensory dependent, plasticity is developmentally restricted, and change is sustained.[3,36,37] Larvae that experienced asymmetric visual input maintained a preferred turn direction for up to 2 weeks post fertilization, approximately 168 h post initial testing (Figures S2D–S2F), extending previously reported findings that did not control visual experience,[26] demonstrating a sustained sensory-dependent effect on motor asymmetry (turn bias direction). We next wanted to establish that the observed plasticity was photo- and not proprio-sensitive. If photic signals induce turn bias direction, then we expect a correlation with light source position versus no correlation if proprioceptive signals were driving plasticity. Indeed, we observed the expected changes in motor asymmetry whether we rotated the source light in the CP assay (Figures 1I and S2G–S2I) or mounted larvae upright with a light source positioned to the side (Figures S2J–S2M). These data show that visual experience instructs turn bias direction.

Next, we wanted to establish whether the observed plasticity was consistent with a CP. Above, we demonstrated that the CP assay imposes motor asymmetry direction through much of larval development. The additional key criterion for CP plasticity is that imposed changes are sensory dependent and developmentally restricted.[3,36,37] To address these other criteria, first, we prepped larvae in the CP assay in constant darkness, but only during the embedding period. The absence of light during the CP completely abolished turn bias modulation (1-way ANOVA, $F(2,123) = 1.86$, $p = 0.16$) but did not disrupt overall motor asymmetry (e.g., did not disrupt match index or total turning) (Figures 1J and S2N–S2P). Next, we examined whether controlling visual experience at later developmental stages would impact turn bias by performing the CP assay from 4–6 dpf. Contrary to early asymmetric visual experience, an asymmetric visual experience later in development did not induce shifts in turn bias performance (1-way ANOVA, $F(2,95) = 0.57$, $p = 0.57$) (Figures 1K and S2Q–S2S). Furthermore, shorter embedding intervals through 2–4 dpf were insufficient to induce turn bias direction (Figure S3). Collectively, our experiments establish

that turn bias direction during search behavior is driven by asymmetric visual experience during an early developmental CP (Figure 1L). Visual experience during the zebrafish visual CP results in sustained behavioral change that is sensory dependent and developmentally restricted, mirroring features in established ODP models.

Asymmetry-maintaining neurons (AMNs) are GABAergic thalamic neurons

Our next goal was to explore the circuit-level mechanisms that support this CP. Previously, we identified approximately 60 neurons genetically labeled by the *Tg(y279:Gal4)* enhancer trap that respond to the loss of illumination and, following bilateral ablation, cause a loss of persistent motor asymmetry, but other search motor patterns remain intact.[26] Here we refer to these neurons as AMNs. Because AMNs underlie the maintenance of motor asymmetry, these neurons are ideal candidates for modulating behavior in a sensory-dependent manner. Initially, we postulated that AMNs reside in the anterior lobe of the posterior tuberculum, based on available zebrafish brain atlas resources.[26,27] However, based on a combination of genetic and circuit structure evidence, we now propose that these neurons reside in the anterior thalamus. Recent studies in larval zebrafish have demonstrated that the s1020t Gal4 enhancer trap labels the anterior thalamus, which is positioned immediately posterior to the zona limitans intrathalamica (ZLI).[38] In addition, subsets of zebrafish thalamic neurons project and transmit illuminance information to the habenula and tectum.[39,40] AMNs are also positioned posterior to the ZLI, and using a current zebrafish single-neuron atlas and neuroanatomy tools, we show that AMNs overlap with the 1020t Gal4 driver and that neurons consistent with this thalamic region project to the habenula and tectum[39,40] (Figures S4A–S4D). Our previous experiments show that a subset of y279-positive AMNs extend projections to the habenula, consistent with other reports describing thalamic projections from this region.[26] Last, the teleost anterior thalamus is composed predominately of GABAergic neurons.[38] Using HCR (hybridization chain reaction) probes against GAD1B, GAD2, and VGlut2b, we identified that nearly all AMNs and surrounding neurons are GABAergic (>95% AMNs expressing GAD1B or GAD2), with few potentially excitatory glutamatergic neurons (<2% AMNs expressing VGlut2b) (Figures 2 and S4E–S4H). Therefore, based on several lines of evidence, the y279-positive AMNs are anterior thalamus neurons.

Thalamic asymmetries correlate to motor asymmetry

Because a persistent motor asymmetry is observed, we posited that an underlying functional asymmetry is required to support this behavior. Our prior studies established that y279-positive AMNs maintain motor asymmetry and respond to changes in illumination, but no correlated asymmetries in neuron function were found that would suggest a direct instructive role.[26] In these earlier studies, a mosaic labeling strategy was used, which may have missed a behavioral correlation. Therefore, we performed calcium imaging in a pan-neuronally labeled line in brain sub-volumes, including AMNs and surrounding regions. Imaging was performed on larvae following the CP assay to identify whether AMN activity correlated with motor asymmetry (Figures 3A and 3B). For recordings, we employed two-photon imaging and used a red LED to elicit light-evoked neural responses, which, as we demonstrated previously, allows the recording of light-evoked neural responses[26] (Figure 3C). For calcium imaging, we used the transgenic line *Tg(Elavl3:H2B-GCaMP6f)*

to resolve single-neuron responses.[41,42] We crossed this line into y279:Gal4; upstream activating sequence (UAS):*NfsB*-mCherry (used as an AMN marker) to identify AMNs from surrounding thalamic and non-thalamic neurons. For analysis, single-neuron responses were grouped into four regions based on neuroanatomical markers[43]: lateral thalamus (part of anterior thalamus containing AMNs), greater thalamus, pallium, and posterior tuberculum (PT) (Figures 3D and 3E). The lateral thalamus encompasses the anterior thalamic regions containing AMNs ($y279^+$ and $y279^-$), whereas we use the term "greater thalamus" to refer to the remainder of thalamic neurons medial and anterior to the AMNs. We recorded from a total of 6,233 neurons and detected photo-mediated changes in neural activity across imaged regions (Figure 3F). Across most recorded regions, we detected three different photo-mediated response profiles (OFF responses, ON responses, and OFF-ON responses) that match established retinal ganglion cell (RGC) response types.[35,44] Predominately OFF responses were observed across tested brain regions, except for the pallium, which had minimal photo-driven outputs (Figure S5A). To determine how photo-responsive neurons may establish motor asymmetry, we compared the numbers and positions of light-responsive ON or OFF neurons in the matched or opposed hemisphere relative to the turn bias direction (Figure 3E). Although y279-specified AMN OFF responders showed a significant hemispheric difference in neuron numbers ($\chi^2(1) = 4.698$, $p = 0.0302$), similar distributions of OFF responders were observed across other thalamic populations but at lower overall density (Table S1; Figures 3G and 3H). Therefore, changes in the number of light OFF-responsive neurons is likely a minor contributor to visual plasticity.

Next, we examined whether changes in neuronal response strength paired with turn bias direction. Within the lateral thalamus, 15.2% (179/1,174) of y279-positive AMNs showed an OFF response, which coincides with the onset of motor asymmetry. Interestingly, when grouped based on behavioral performance, we find that y279-positive AMNs show a stronger response in the hemisphere opposed to the turn bias direction (Figure 3I). This analysis was based on a single-neuron comparison across all tested fish; similar trends were observed when we analyzed y279-positive AMN responses on a per-fish basis (all responses averaged per larva) or per behavior (responses from left- and right-biased individuals) (Figures S5B–S5D). To independently confirm the observed AMN responses observed in the pan-neuronal imaging, we injected *Tg(y279:Gal4)* larvae with a UAS:nls-GcaMP6s construct to mosaically and unambiguously label y279-positive AMNs. Using an identical recording strategy as above, the mosaic labeling of AMNs recapitulated the pan-neuronal imaging, confirming the correlation between AMN physiology and turn bias (Figure S5E). Conversely, OFF responses in lateral thalamic y279 negative neurons showed no hemispheric asymmetries associated with behavior (Figure 3J).

We examined whether the functional asymmetries observed in the y279-positive AMNs were specific to the lateral thalamus or a broader feature in the brain. Surprisingly, OFF responses in the greater thalamus (6.1% [140/2,281] of neurons) also showed functional asymmetries that correlated with turn bias direction but displayed increased responsiveness in the hemisphere matched to turn bias, opposite the pattern observed in lateral thalamic y279-positive AMNs (Figure 3K). Contrary to thalamic neurons, OFF response posterior tuberculum neurons (posterior to the thalamus; 310/2,073, 15.0% of neurons) demonstrated no hemispheric asymmetries based on turn bias direction (Figure 3L). We did not explore

pallium functional asymmetries because so few neurons responded to visual stimuli. Our data establish that distinct subsets of thalamic neurons are functionally correlated with motor asymmetry, which was not observed in surrounding brain regions. Together, our data suggest that visual experience changes the strength of OFF-responsive neurons in the thalamus.

Identifying distinct activity patterns in AMNs versus adjacent greater thalamus neurons led us to ask how these populations contribute to turn bias behavior. Previously, we demonstrated, using laser ablation, that unilateral loss of AMNs imposes turn bias toward the intact hemisphere but had no significant impact on baseline motor patterns.[26] Here we utilize targeted laser ablation to perform unilateral ablations of AMNs as a control or adjacent greater thalamus neurons to elucidate their impact on motor performance (Figure 3M). Unablated controls that were similarly prepped as ablated larvae showed no population-level shift in turn bias direction. Moreover, consistent with our prior study,[26] unilateral AMN ablation creates robust turn bias toward the intact hemisphere (contralateral bias). Conversely, ablation of greater thalamus neurons adjacent to AMNs drove an ipsilateral turn bias toward the ablated hemisphere (Figure 3N). Neither AMN nor greater thalamus ablation caused a directional preference during illuminated baseline movement, suggesting a specific impact on turn bias (Figure S5F). Despite both thalamic populations modulating turn bias performance, we noticed that only the unilateral loss of AMNs produced stronger same-direction turning as observed for absolute turn bias (1-way ANOVA, $F(2,93) = 19.57$, $p < 0.0001$) and match index (Kruskal-Wallis test, $H = 19.01$, $p < 0.0001$) (Figures 3O and S5G). AMN ablations resulted in a loss of fluorescence and visible structural deformations consistent with laser ablation,[26,45] which could also be observed to confirm the ablation of greater thalamus neurons (Figure S5H). Altogether, our functional and ablation data show that subsets of thalamus neurons have different sensory-dependent activity patterns and influence on determining the direction and strength of motor asymmetry during search behavior. Moreover, the data suggest that AMN signaling is likely a dominant driver of motor asymmetry.

Thalamic AMN responses are retina dependent

Previously, we showed that RGCs and AMN neurites colocalize in the adjacent neuropil, but whether the retina drives AMN activity was not determined.[26] Based on mammalian ODP models and our behavioral assays in zebrafish, we hypothesize that lateral thalamus photo-responsiveness is retina driven. To test this hypothesis, we perform unilateral enucleations to eliminate visual input from a single eye and simultaneously record thalamic responses to visual stimuli in both hemispheres simultaneously (Figures 4A–4C). In zebrafish, RGCs project exclusively to the contralateral hemisphere;[31,46] therefore, unilateral enucleation eliminates all contralateral photic input. In the lateral and greater thalamus, visually evoked responses are largely lost in the enucleated hemisphere but maintained in the intact hemisphere (Figures 4D and 4E). However, our regional analysis did detect slight calcium responses in the enucleated hemisphere, suggesting that enucleation did not remove all thalamic photo-responsiveness. Because thalamic neuron populations displayed different patterns of visually mediated activity, we examined single-cell responses across the thalamus in our unilaterally enucleated preps. Abolishing RGC input reduced, but did not eliminate, photo-responsive neurons in the enucleated hemisphere (comparisons between hemispheres:

greater thalamus, $\chi^2(1) = 7.410$, $p = 0.0065$; lateral thalamus y279$^+$, $\chi^2(1) = 17.067$, $p < 0.0001$; lateral thalamus y279$^-$, $\chi^2(1) = 4.765$, $p = 0.0290$) (Figure S5J). The remaining OFF-responsive AMNs (y279$^+$) displayed lower peak activity compared with the intact hemisphere, whereas the GCaMP signal in the greater thalamus and y279$^-$ lateral thalamus neurons were similar between hemispheres (Figures S5K–S5M). However, the low number of responsive neurons in the enucleated hemisphere likely reduces the power of statistical comparisons. Nonetheless, some photic information to the thalamus is RGC independent. Because visual experience is needed to impose turn bias direction (Figure 1), and there are relatively few of these RGC-independent neurons, we reason that this input has a nominal role in plasticity. Yet, RGC-independent responses could be a source of inter-hemispheric regulation. Overall, our data show that thalamic responses are largely dependent on contralateral retinal input. Because RGCs are predominately glutamatergic, we next expressed the glutamate sensor iGluSnfer[47] in AMNs and recorded from the adjacent neuropil in unilaterally enucleated larvae (Figures 4C and 4F). Indeed, we found glutamatergic activity following loss of light from the intact but not enucleated neuropil (Figure 4F). As a control, we quantified iGluSnfer responses in a posterior neuropil position distant from potential RGC inputs. The posterior neuropil showed no evidence of visually evoked glutamatergic signaling, suggesting that our AMN-adjacent neuropil is a region of RGC-dependent glutamatergic release (Figure S5N). Our prior experiments establishing the proximity of RGC and AMN neurites in combination with our current experiments suggest that AMNs are receiving visual OFF signals from RGCs but do not unambiguously support direct RGC innervation.

Because the thalamus receives RGC input, a potential caveat is that thalamic asymmetries are driven by a sustained retinal output asymmetry created by the imbalanced visual experience during the CP assay, a putative retina plasticity model. Because we observe different patterns of functional asymmetry across the thalamus (e.g., lateral vs. greater thalamus; Figure 3), we consider this outcome unlikely. Nevertheless, we recorded activity in the optic tectum neuropil, where RGCs directly innervate, following changes in illumination (Figures 4G and 4H). The optic tectum is the primary visual processing center in zebrafish and receives the majority of RGC input.[48] Unlike AMNs or the greater thalamus, optic tectum neuropil responses across hemispheres show no differences based on turn bias direction (e.g., symmetric across hemispheres) (Figures 4I–4J). These data indicate that thalamic responses depend on the retina. However, we only observe functional asymmetries correlated with turn bias in the thalamus and not in visual processing centers, excluding a retina-centric plasticity model. Therefore, sensory experience during the CP instructs sustained functional changes in the thalamus.

GABAergic signaling maintains zebrafish CP timing and is necessary for thalamic asymmetries

Shifts in the developmental window for CP plasticity can be induced by pharmacologic manipulation of GABAergic activity,[10,18,24] showing that the timing of GABAergic circuit development is a fundamental mechanism for regulating ODP. A recent *Drosophila* study also identified a CP for motor behavior, which similarly requires inhibitory signaling,[49] suggesting that inhibitory signaling is an essential and conserved mechanism in CP

regulation, regardless of cortical input. To test whether GABAergic signaling is necessary for zebrafish ODP, we used pentylenetetrazol (PTZ), a reversible non-competitive antagonist of $GABA_A$ receptors.[50] In zebrafish, high concentrations of PTZ induce seizures, resulting in clonus-like convulsions and epileptiform brain discharges.[51,52] To treat zebrafish during the entire CP and avoid severe dysregulation of neural activity, we used 1 mM PTZ, which is below concentrations reported to induce seizures,[51] and treatments to maintain grossly normal motor behavior and motor asymmetry (Figures S6A–S6C). To confirm and quantify activity changes, we developed a fluorescent *in situ* hybridization probe to detect changes in c-fos expression, a well-established marker for increased activity in zebrafish.[53–56] Using a high dose of PTZ, we confirmed that our HCR c-fos probe would detect increased neural activity (Figures S6D and S6E).

Low-dose PTZ treatment during the zebrafish visual CP blocks sensory-dependent modulation, resulting in no population level induction of turn bias direction (1-sample t test to 0, right side down [RD]: $t(30) = 0.50$, $p = 0.62$; left side down [LD]: $t(29) = 0.86$, $p = 0.40$) (Figures 5A and S7A–S7C). Cotreatment with muscimol, a non-competitive $GABA_A$ agonist,[57,58] restores plasticity, suggesting a GABA-specific effect (1-sample t test to 0, RD: $t(26) = 0.37$, $p = 0.04$; LD: $t(25) = 2.34$, $p = 0.03$) (Figures 5A and S7D–S7F). Interestingly, this rescue was not observed using gaboxadol, an extra-synaptic GABAergic agonist[59–61] (Figures S7G–S7I). To confirm that the loss of plasticity is GABA specific and not a by-product of altered neural ctivity, we treated larvae during the CP assay with 4-AP (a voltage-gated potassium channel blocker) or caffeine (an adrenergic receptor agonist) to stimulate neural activity,[62,63] which we confirmed using HCR c-fos labeling (Figures 5B–5D and S7J–S7L). Despite increases in neural activity, neither 4-AP nor caffeine blocked turn bias induction following asymmetric visual experience (Figure 5B). These results support our prior experiments showing $GABA_A$-specific regulation of zebrafish visual plasticity. In mammals, disruption of GABAergic signaling delays CP onset,[24] but whether this mechanism is specific to the cortex and/or thalamus is unknown. Therefore, using our thalamuscentric zebrafish model, we next asked whether GABAergic inhibition abolished plasticity or caused a delay in CP onset. To determine how GABAergic signaling affected the CP, we PTZ-treated free-swimming larvae during the established CP (2–4 dpf), removed the drug, and performed delayed embedding in the CP assay from 4–6 dpf. Untreated control larvae showed no plasticity following the 4–6 dpf CP assay, consistent with prior experiments (Figure 1K). Conversely, following GABAergic inhibition, the period for sensory-dependent plasticity was shifted, resulting in visual plasticity at later developmental stages (Figure 5E). Our data show that (1) GABAergic signaling is necessary to establish CP timing in zebrafish, (2) synaptic GABAergic receptors are specifically required, and (3) the role of inhibitory signaling is likely conserved across vertebrates and invertebrates.

Our data imply that thalamic inhibitory signaling contributes to CP timing, suggesting an impact on thalamus function, which we investigated next. To determine whether inhibitory signaling was contributing to CP timing and photo-dependent modulation of thalamus neuron activity, we PTZ-treated larvae in the CP assay from 2–4 dpf and performed calcium imaging at 4 dpf (Figures S8A and S8B). Our behavioral data show that the window of plasticity is extended by GABAergic inhibition; therefore, we hypothesized that, at 4

dpf, functional differences between hemispheres should be observed in the control but not following inhibition of GABAergic signaling. We recorded from a total of 1,6921 neurons (control: N = 19 larvae, 8,106 neurons; PTZ treated: N = 19 larvae, 8,815 neurons) and, similar to later stages, found predominately light-OFF responses across recorded brain regions (Figure 5F). PTZ treatment resulted in an increase in OFF-responsive AMNs (lateral thalamus y279^{+} neurons) compared with untreated controls ($\chi^2(1) = 12.509$, $p = 0.0004$), which was not observed in surrounding regions (lateral thalamus y279^{-}: $\chi^2(1) = 0.643$, $p = 0.4228$; greater thalamus: $\chi^2(1) = 0.655$, $p = 0.4182$; PT: $\chi^2(1) = 0.3592$, $p = 0.3592$). For functional comparisons, we grouped neuronal responses as matched or opposed based on larva positioning in the CP assay and expected turn bias direction (Figure 1L). In untreated 4-dpf control larvae, AMN OFF responses displayed functional asymmetries consistent with later development stages (e.g., larger opposed hemisphere response) (Figure 5G). This observation supports our behavioral data showing that the visual CP ends at 4 dpf and our prior work demonstrating that turn bias is detectable by 4 dpf, suggesting that visual experience-dependent changes are largely ingrained in the brain by this developmental stage.

Conversely, attenuated inhibitory signaling during the CP abolishes the peak OFF-response differences in AMNs based on CP assay positioning, supporting our hypothesis and consistent with a loss of sensory-mediated change (Figure 5H). Unlike later-stage larvae, we observe no differences in peak OFF-responses in the greater thalamus in either control or PTZ-treated larvae. Similar to later developmental stages, lateral thalamus y279^{-} and PT OFF responses showed no hemispheric differences in peak responses (Figures S8D–S8I). In PTZ-treated larvae, we note a delayed and sustained increase in matched hemisphere activity across most brain regions tested (Figures 5H, S8H, and S8I). We posit that this is a by-product of PTZ treatment, which, even at the low concentrations used here, causes increased turning behavior and turn bias (Figure S6B). Our data establish that inhibitory signaling during the CP is necessary for behavioral and thalamic functional changes to arise in response to visual experience.

Activation of AMNs sufficient to drive motor responses

Next, we wanted to determine how thalamic AMNs affect motor behavior. We focused on AMNs because this population had more OFF-responsive neurons (Figures 3; Table S1). Based on our functional imaging, we hypothesized that AMNs could modulate motor performance through two possible mechanisms: (1) asymmetric inhibition or (2) asymmetric disinhibition. We consider the first mechanism unlikely. Even though the stronger GABAergic AMN responses are observed in the hemisphere opposed to turn bias direction, supporting an asymmetric inhibition model for the observed turn biases, we demonstrated previously that unilateral ablation of AMNs imposes a turn bias toward the intact hemisphere (away from the ablated hemisphere).[26] Therefore, if AMNs controlled motor behavior through asymmetric inhibition, then a turn bias toward the ablated side would be expected and was not observed.[26] Therefore, we used optogenetic tools to directly manipulate AMN activity to address whether AMNs modulate motor performance using disinhibition. We injected y279 larvae with a UAS:ChEF-v2a-mCherry driver for optical stimulation,[64] UAS:TagRFP-v2a-paGFP (used only for TagRFP expression) as a control, or UAS:GtACR2-tdTomato for optical inhibition.[65] Because the y279 line labels neurons in

addition to AMNs[26,27](Figure S3), we used a two-photon laser to photo-stimulate AMNs with three-dimensional precision while simultaneously recording tail movement as a readout of motor responsiveness (Figure 6A). We have shown that both brain hemispheres can support motor asymmetry using unilateral ablation[26] and that expression of the optogenetic drivers is mosaic, so we bilaterally stimulated AMNs because interpreting hemisphere-specific stimulation would be challenging. Because two-photon lasers are tunable to specific wavelengths, we performed a stimulation series on each larva, including a baseline (no laser), stim-ʎ off-peak (1,040 nm two-photon [2P]/520 nm at cells), and stim-ʎ on peak (940 nm 2P/470 nm at cells) (Figure 6B). If AMNs modulate motor behavior using disinhibition, then we expect direct activation of AMNs to release motor activity (tail movement) in our preps. Indeed, larvae expressing the optogenetic activator ChEF, exposing AMN neurons to stim-ʎ on peak (940 nm) evoked tail movement, which was not observed during baseline or off-peak laser exposure (1-way ANOVA, $F(2) = 54.93$, $p < 0.0001$) (Figures 6C and 6D). Across all photo-stimulation intervals, no significant tail movement was observed in controls or larvae expressing the optogenetic inhibitor GtACR2 (Figures 6E–6H). We confirmed that our 2P stimulation paradigm did not result in neuronal death (Figures S8J and S8K), suggesting that motor changes were due to optogenetic stimulation. These data show that thalamic AMNs can affect motor activity by disinhibiting downstream motor control pathways.

DISCUSSION

We demonstrate a thalamus-centric visual CP in larval zebrafish that recapitulates hallmarks of mammalian ODP. Asymmetric visual experience in zebrafish imposes asymmetries in the thalamus, providing a neuron-level functional analysis of ODP-driven changes in thalamus neurons. In mammals, the thalamus receives significant cortico-thalamic feedback, and isolating thalamic changes requires extensive manipulation.[21,22] Conversely, zebrafish lack a cortex,[66] eliminating cortical feedback. Therefore, zebrafish are a robust model for establishing foundational subcortical plasticity principles.

In zebrafish, experience-dependent changes in the nervous system are well documented. In the optic tectum, environmental light is necessary to shape tectal activity patterns.[67,68] One study suggests a 5–7 dpf CP for tectum functional development[67] but does not examine asymmetric visual experience. Asymmetric visual experience has been investigated in *Xenopus* tadpoles, where it drives changes in isthmic-tectal communication;[69] the tectum is the homolog of the superior colliculus.[70] In mammals, minimal ODP has been described in the superior colliculus.[71] In larval zebrafish, we did not observe functional asymmetries in the optic tectum, nor did we observe functional asymmetries outside of the thalamus. In zebrafish, the thalamus controls various photo-mediated responses.[39,40] Because only a subset of $y279^+$ thalamic neurons responded to the light-OFF stimulus, neurons across the thalamus are likely tuned to specific photic cues. Indeed, a subset of thalamus neurons projects to the tectum and regulates loom-induced startle in zebrafish,[40] and in mammals, portions of the thalamus respond to illuminance to control defensive behavior.[72] Previously, we did not observe AMNs extending to the tectum,[26] supporting the hypothesis that the zebrafish thalamus is divided into unique photo-responsive regions, suggesting that AMNs operate in a tectum-independent manner, consistent with our current results.

Comparison with mammalian plasticity

Despite the benefits of zebrafish as a model, there are differences compared with mammalian ODP. Changes in binocularity contribute to the functional shifts observed in mammals during ODP.[4,19,37,73,74] Conversely, zebrafish RGCs project to the contralateral hemisphere, providing only monocular input.[31,75] However, RGC input to the mammalian thalamus is predominately monocular.[21,23] Therefore, pertinent ODP changes in zebrafish are also likely occurring in the thalamus despite differences in binocularity. The neuronal composition also differs between species. In mammals, excitatory relay neurons in the dorsal lateral geniculate nucleus (dLGN) are the primary thalamic retinorecipients that project to the visual cortex, and these projections within the cortex have been the primary target for functionally characterizing thalamic ODP.[21,23] A subset of inhibitory dLGN interneurons also receives RGC input,[37,74] but ODP changes have not been tested. Conversely, the zebrafish thalamus is predominately GABAergic but is also a retinorecipient target.[38,48] Our previous and current work suggest that AMNs likely receive RGC input. Therefore, in zebrafish, ODP changes are likely focused on GABAergic neurons because of the lack of a cortex and putative need for a relay neuron homolog. In zebrafish, a clear LGN homolog has not been identified.[38] An attractive hypothesis is that AMNs in the lateral zebrafish thalamus serve, at least partially, as an LGN homolog, but this hypothesis requires further testing.

Mechanism of thalamic ODP—Our data suggest that OFF responses are primarily affected by ODP-like manipulation in the zebrafish thalamus and that the AMN OFF responses are reduced in the hemisphere ipsilateral to the stimulated eye compared with the contralateral hemisphere (light-deprived eye). Interestingly, we observe the opposite effect in greater thalamic neurons. Our ablation experiments show that these neurons support ipsilateral turning. However, fewer OFF responses are observed in the greater thalamus, which also have a weaker drive on behavior relative to AMNs, based on laser ablation results, suggesting a less influential role. However, our imaging experiments suggest that functional asymmetries in the greater thalamus develop later than in AMNs. An interesting hypothesis is that greater thalamus asymmetries form later to maintain AMN asymmetries. We also establish that, just like ODP in the cortex,[18,24] thalamic changes require GABAergic signaling to allow experience-dependent modulation of neuron responsiveness and determine the timing of CP plasticity. In addition, inhibitory signaling during the CP is necessary for AMN functional asymmetries to develop. Interestingly, GABAergic inhibition only resulted in an increase in the number of OFF-responsive AMNs, suggesting that inhibitory signaling may refine the AMNs responding to loss of illumination to support or maintain hemispheric differences, but this hypothesis will require further testing. We demonstrate that activation of AMNs is sufficient to evoke motor responses, suggesting a direct ability to impact motor performance. Nonetheless, these divergent patterns of activity within the thalamus imply that Hebbian (AMNs) and homeostatic (greater thalamus) plasticity mechanisms could be occurring, consistent with the multiple forms of plasticity occurring during mammalian ODP.[76–78] What remains unknown is whether these changes happen at retino-thalamic inputs, intrinsically within thalamic neurons, or in associated inhibitory circuits. Our data show increases in the strength of OFF response y279^{+} AMNs in the hemisphere opposed to the turn bias direction and an opposite response profile in adjacent neurons in the greater thalamus, suggesting multiple forms of plasticity in

the zebrafish thalamus. Regardless of how plasticity occurs, we propose a model where GABAergic AMNs regulate motor performance by a disinhibition model (Figure 7). Our previous work demonstrated that unilateral ablation of AMNs imposed a turn bias toward the intact hemisphere,[26] implicating that a contralateral projection needs to exist for our model to work. AMNs may inhibit contralaterally projecting premotor inhibitory neurons, which inhibitory glycinergic neurons have been described in the zebrafish hindbrain that regulate motor behavior and predominately inhibit contralateral neurons.[79–81] Alternatively, ipsilaterally projecting glycinergic neurons are also present in the zebrafish hindbrain, and future tracing experiments could demonstrate that AMNs project contralaterally, leading to the same behavioral effect.

In the mammalian cortex, populations of parvalbumin, VIP^+, and sst^+ GABAergic neurons have well-established roles in plasticity.[82] Similarly, the neurotrophic factor BDNF has a critical role in GABAergic neuron maturation and an essential role in modulating CP plasticity.[83,84] Indeed, numerous molecular pathways, including calcium-dependent signaling, cannabinoid receptor signaling, and gene expression regulation, have defined roles in regulating the visual CP and cortical plasticity.[85–87] Conversely, thalamic molecular mechanisms instructing CP regulation or visual-experience-dependent changes are incompletely understood. Our current study and others have established that GABAergic signaling is required for thalamic plasticity, illustrating a conserved role of inhibitory signaling between cortical and subcortical regions.[20] However, different brain regions show varying requirements for GABA receptor composition because only thalamic plasticity requires GABRA1 containing receptors despite also being expressed in the cortex.[20] Therefore, moving forward, two exciting lines of experimental inquiry may target potential combined cortex and thalamus or tissue-specific molecular mechanisms for plasticity. To this end, our zebrafish model offers several advantages for molecular manipulation with tools for tissue-specific manipulation, high-throughput CRISPR knockdown, and extensive transgenic drivers.[88–91]

ODP regulation of search behavior—Previously, we demonstrated that the direction of motor asymmetry is not inherited, suggesting a role of environmental determinants.[26,27] Recently, we published a screen of etiologically relevant environmental factors, showing that turn bias direction can be modulated by environmental experience. However, we did not elucidate a causative factor imposing left or right turn bias during search behavior.[27] Here we show that asymmetric visual experience instructs this outcome. Interestingly, the CP interval is largely before swim bladder inflation, when larvae are predominately on their side.[92] Therefore, larvae may naturally receive asymmetric visual input during this time, producing an environmental mechanism equivalent to the CP assay. Because larvae would typically be positioned randomly in their environment, this model also explains the equal distribution of left versus right turners observed, providing a mechanism to generate randomness at the population level, which randomness and behavioral unpredictability has evolutionary advantages.[93–95] However, even following the CP assay, we note that a subset of individuals shows motor asymmetry opposed to the expected turn bias direction, based on CP assay orientation. This divergence could result from natural variation driving unique individualistic responses.[96,97] Alternatively, in our CP assay, the “occluded” eye

likely receives some visual input. In mammalian ODP experiments, an eye is typically surgically sutured to completely block visual experience. In our model, we benefit from avoiding surgical manipulations that could prompt inflammation and potentially interfere with plasticity,[98] but this incomplete blockage may cause some behavioral noise in our experiments. A benefit to this approach is that future studies can address how changes in photo-stimulation during the CP affect plasticity, which would be challenging with surgical occlusion methods. Our work collectively establishes a powerful vertebrate model to interrogate how visual experience modulates subcortical thalamic circuits and behavioral performance. Here we used this model to demonstrate neuron-level functional changes in the thalamus and implicate thalamic control of CP onset through inhibitory signaling.

Limitations of the study

The structure of the zebrafish visual system offers simplicity but cannot address changes in binocular integration. Similarly, the neuroanatomy of zebrafish allows thalamic changes to be studied directly, which also negates being able to address mechanisms that integrate signals across cortical and subcortical regions. Moreover, in larval zebrafish, we cannot suture or readily patch an eye to unambiguously exclude all photic input. Therefore, even the occluded eye in our model may receive partial or intermittent visual input. Not completely blocking visual stimulation may cause some of the noise observed in our model (e.g., turn bias opposed to that expected from the CP assay) but may also allow assays that modulate visual experience in therapeutically relevant manners without successive surgeries. Last, an ideal experiment would show functional changes while simultaneously recording behavior. Larval zebrafish are amendable to such experiments, although typically address rapid evoked responses like visual or acoustic startle. Previously, we described that head-embedded larvae, a typical prep for imaging, do not generate sustained responses to reliably indicate turn bias.[26] Nonetheless, we show that individual turn bias is sustained and that the correlation between turn bias and thalamic asymmetries is robust (Figures 3 and S5).

STAR★METHODS

RESOURCE AVAILABILITY

Lead contact—Further information and requests for resources and reagents should be directed to the lead contact, Eric Horstick (eric.horstick@mail.wvu.edu)

Materials availability—The study did not generate new unique reagents and materials.

Data and code availability—This study did not report original sequencing data or code. Any additional information required to reanalyze the data reported in this paper is available from the lead contact upon request. Data can also be accessed through Mendeley Data: https://doi.org/10.17632/bpj99zrshg.1.

EXPERIMENTAL MODEL AND SUBJECT DETAILS

Zebrafish husbandry—All experiments were approved by the West Virginia University Institutional Animal Care and Use Committee. Adult Tübingen long-fin (TL) zebrafish (*Danio rerio*) were used as a genetic background for all experiments. All experiments

were performed within 14 days post fertilization (dpf) before sex determination. Larvae were raised at 28°C on a 14/10 h light-dark cycle at 75 μW/cm^2 intensity, in embryo media 3 (E3: 5mM NaCl, 0.17mM KCl, 0.33mM $CaCl_2$, 0.33mM $MgSO_4$-7H_2O, and 1mM HEPES buffer pH 7.5) at a raising density of 40 larvae per 30mL E3 unless stated otherwise. Transgenic lines used were *Tg(y279: Gal4)*,[26] *Tg(UAS:Kaede)s1999t*,[99] *Tg(UAS:nsfB-mCherry)*,[99] *Tg(elavl3:H2B-GCaMP6f)*,[41] *Tg(elavl3:GCaMP6f)*.[106]

METHOD DETAILS

Behavior tracking and analysis

Trajectory analysis: Larvae were recorded at 10 Hz using a μEye IDS1545LM-M CMOS camera, using infrared illumination (940nm, CMVision Supplies), and tracked using DAQtimer and custom software. Individual larvae were placed in 6-cm petri dishes and tracked over four simulation series of 30 s baseline illumination immediately followed by 30 s following the loss of illumination, with each recording set separated by 150s of untracked baseline illumination. We used three measures to establish motor behavior: Match Index, Total Turn Angle (TTA), and Bias Ratio (BR). *Match Index*: Proportion of trials that match the direction of the first dark trial bias. Individuals who have a rightward bias on the first trial and leftward bias on the subsequent trials would have a match index of 0, while individuals who have four trials of rightward bias would have a match index of 1. *TTA*: The sum of all angular trajectories regardless of direction. *BR*: The net turn angle is the sum of all angular trajectories with respect to direction (left turns being negative degrees change, while right turns are positive degrees) divided by the TTA. Therefore, individuals who only turn rightward will have a BR of 1, while those who only turn leftward will have a BR of −1. If an individual has an equal magnitude of leftward and rightward turns in a tracking period, their BR would be 0. Trials that had less than 10s of data were excluded from analyses. Individuals missing >2 baseline or >1 dark response(s) were excluded. Individuals missing the first dark trial were excluded from Match index calculations.

Critical period assay: For CP assay experiments, larvae were raised under standard conditions before, during, and after embedding. At 2 dpf larvae were manually dechorionated using forceps. Individuals were lightly anesthetized using dilute Tricaine (Sigma) until touch unresponsive and mounted in 1% low melting temperature agarose for all CP assay experiments. For embedding at later developmental stages (4–6 dpf) agarose was cut away from the mouth and gills to allow for adequate oxygenation and ion exchange. A 25% neutral density filter was placed under dishes to provide greater contrast between the eyes. For CP assay involving lack of visual stimulus, mounted individuals were kept in a blackout box. For the light-rotated visual stimulation CP assay, individuals were mounted on the inner lid of a Petri dish with a neutral density filter placed on top of the dish and illuminated from below. Following removal from agarose, individuals were raised under normal conditions, and behavior was tested at 6–7 dpf for 2–4 dpf embedding and 9 dpf for 4–6 dpf embedding unless stated otherwise. To assess the level of asymmetric visual experience during the CP assay, individuals were laterally embedded in low melting temperature agar at 4dpf similar. We used a 455 nm LED (ThorLabs) at 10 μW/cm^2 narrowed using a pinhole to a beam approximately the diameter of the larval eye. Using an optometer (International Light Technologies Model 2400 Optical meter), we measured

light depression through the agar immediately adjacent to the larvae, the tail, and the eyes. Measures were standardized to the light intensity through the agar alone. For embedding larvae upright and providing a lateral light source. A black aryclic bar was glued to the center of a Petri dish and larvae were agar embedded along the sides of the bar. LED arrays were symmetrically positioned on either side of the Petri dish and experiment was carried out similar to typical CP assay experiments.

Extended timeline: Larvae were mounted and behavior tested as described above. Following behavior testing at 6–7 dpf, individuals were raised in our fish facility in system water. Larvae were raised in 300 mL of system water initially, with 200 mL added daily until 12 dpf where they were put on a slow drip water flow (~1 drop/sec). Babies were fed 75 micron GEMMA until 12 dpf, when they transitioned to 150 micron GEMMA. Individuals were behavior tested at 14 dpf as described above, except using system water versus E3.

Pharmacology—Neural activity was modulated using pentylenetetrazole (PTZ, Sigma, P6500), muscimol (Sigma, M1523), caffeine (Sigma, C0750), 4-aminopyridine (4-AP, Sigma, 275875), and gaboxadol (Sigma, T101). Stocks were prepared in molecular grade water. To test the impact on turn bias, larvae were treated with each drug diluted in E3 to working concentrations. The CP assay was conducted as previously mentioned. Drugs were replaced daily for all experiments. At 4 dpf, the drug(s) were removed, and fresh E3 was used for the rest of the experiment.

Labeling experiments

***Fluorescent* in situ *hybridization*:** Molecular Instruments HCR fluorescent *in situ* hybridization technology was used for all gene expression experiments. Company designed probe sets were generated based on provided accession numbers for GAD1b (NM_194419; 17 probes), GAD2 (NM_001017708; 20 probes), and VGlut2b (NM_001009982, 17 probes). A company-validated kaede probe set (17 probes) was ordered to label AMNs in *Tg(y279:Gal4; UAS:Kaede)* larvae. At 3dpf, *Tg(y279:Gal4; UAS:Kaede)* larvae were fixed overnight at 4°C in 4% paraformaldehyde in 1x PBS and 0.1% Tween 20. After fixation, embryos were washed in 1x PBS with 0.1% Tween 20, and labeling was conducted using HCR RNA-Fish protocol (Hageter et al. 2021). Imaging was performed on an Olympus Fluoview FV1000 confocal using a 40x oil immersion objective. To measure changes in brain activity, a fosab/c-fos (NM_205569, 27 probes) probe was designed by Molecular Instruments. Larvae were drug treated for 1 h at 4dpf. Following treatment, larvae were fixed and labeled for fosab. Images were captured on a ThorLabs Confocal with a TOPTICA iChrome CLE 50×laser and 20× objective using consistent laser power and gain settings across all samples. A consistent plane in the brain was captured for all larvae. For analysis, the whole brain area mean intensity was quantified using ImageJ and standardized to control larvae.

Cell counting: Cells were counted using confocal stacks of AMNs from fixed 3dpf *Tg(y279:Gal4; UAS:Kaede)* larvae labeled using fluorescent in HCR FISH to detect kaede mRNA and GAD1b, GAD2, or VGlut2b RNA expression. Kaede labeling was used to

identify individual AMNs, which were manually assessed for expression of other markers within the kaede-expressing AMNs.

Pixel colocalization: To provide a supporting quantitative measure of colocalization pixel colocalization counts were collected for each individual that underwent manual cell counting for colocalization. Each AMN was first outlined in ImageJ to act as an ROI. The analysis tool "Colocalization Threshold" in ImageJ was used to compare kaede positive pixel placement with kaede to GAD1b, GAD2, or VGlut2b positive pixels to calculate percent colocalization.

Functional imaging

Calcium imaging: Calcium imaging was performed across whole single planes, using *Tg(y279*: *Gal4)*; *Tg(UAS*:*nsfB-mCherry) or (UAS*:*epNTR-tagRFPt)*; *Tg(elavl3*:*H2B-GCaMP6f)* or *Tg(elavl3*:*GCaMP6f)* for nuclear-localized or regional calcium recording, respectively. Larvae were raised in 200μM PTU from 1 dpf until 24 h before imaging. Behavior was run to confirm turn bias direction at 6 dpf. For enucleation experiments, larvae were anesthetized and unilaterally enucleated at 5 dpf in 1x Evans and returned to E3 approximately 24 h post-enucleation. For nuclear-localized calcium imaging, larvae were mounted in the CP assay. At 7 dpf, larvae were lightly anesthetized using tricaine and mounted in 2% low-melting temperature agarose. Experiments were performed using a Scientifica Vivoscope two-photon, a 16x water immersion objective, and Spectra-Physics MaiTai laser tuned to 980nm. Visual stimulation was provided using a Thorlabs mounted 660-nm LED at 70 μW/cm^2. For each larva, a 1-min light ON, 1-min light OFF, and 1-min light ON stimulus series was repeated twice per larva with a 3-min red light ON interval between replicates. Stimulation series were preceded by 5 min of constant red light illumination to adapt larvae. We captured a single plane of the thalamus using *Tg(y279*: *Gal 4*; *UAS*: *nsfB-mCherry)* as a guide for AMNs and surrounding brain regions. We chose a single plane based on neuroanatomic structure for imaging the optic tectum. Image acquisition was performed using ScanImage software at ~1.01 Hz. All images were registered using the TemplateMatching plugin for ImageJ.[107] For nuclear-localized calcium imaging, we analyzed fluorescence intensity changes by manually drawing an outline of each cell and extracting mean gray values from those ROIs using a sum projection and the Romano-et-al toolbox in MATLAB. A custom program was written in MATLAB to calculate $(F_t - F_0)/F$, ($\Delta F/F$), where F_0 was the mean gray value during the baseline period. Neurons with an $\Delta F/F$ greater than 3 standard deviations of the baseline for 3 successive frames following complete light extinction were classified as OFF-responses, following the return of illumination, ON-responses, and both OFF/ON-Responses. Cells were categorized into regions based on localization and using Mapzebrain regions.[43] Using a composite image of GCaMP6f and the y279 reporter, cells were classified to either be y279 positive or negative. Analysis for regional recordings was performed by outlining ROIs in ImageJ and using the "plot z axis profile" function to extract gray values and calculate $\Delta F/F$ in Excel. For mosaic calcium imaging, embryos at the single cell stage were injected with 20 pg of UAS:NLS-GCaMP6s[26] plasmid and co-injected with 25pg of tol1 mRNA. Larvae were raised, behavior tested, imaged, and analyzed as above.

***4dpf PTZ calcium imaging*:** Larvae were raised in 200μM PTU starting at 1 dpf, mounted in the standard CP assay and treated with PTU alone or 1mM PTZ, and the PTU and PTZ were refreshed daily until 4dpf. Individuals were given 1–2 h out of PTZ and PTU before calcium imaging and imaged at 4dpf. Imaging was acquired as described above. Regions were designated and analysis performed as described above for later stage calcium imaging.

iGluSnfer: Single-cell stage *Tg(y279*:*Gal4*; *UAS*:*nsfB-mCherry)* embryos were co-injected with 20 pg of UAS: 14xUAS-iGluSnf[102] and 25 pg of tol1 mRNA. Larvae were raised in 200μM PTU from 1 dpf −5dpf and enucleated at 5 dpf. Larvae were mounted and imaged, similar to the calcium imaging experiments. Images were captured at 2.00 Hz. We calculated $\Delta F/F$ from a region lateral to the y279 reporter in the adjacent neuropil and a posterior position as a control.

Laser ablation—*Tg(y279*:*Gal4*; *UAS*:*Kaede)* embryos were raised with 200 μM PTU until 4dpf. At 4dpf, larvae were immobilized with a low-dose of tricaine, mounted in 2% low-melt agarose, and imaged with a Scientifica two-photon Vivoscope with Spectra-Physics MaiTai laser and 16x water immersion objective. Image acquisition was performed with ScanImage software through MATLAB. For representative imaging, laser wavelength was tuned to 940 nm with a power of 15 μW. Representatives were captured at a 7x zoom with a single plane scan through the AMNs. Ablations were conducted with successive 2 s acquisitions at 70x zoom with the laser power set to 80 μW. Successful unilateral AMN and medial thalamic neuron ablations were determined by the near-complete loss of fluorescence or development of tissue scarring (cavitations and obvious tissue distortion), respectively. Any medial ablation resulting in significant damage to the proximal AMNs in the lateral thalamus or opposing hemisphere were excluded. Post-ablation individuals were raised in 1x Evans solution until 5dpf and subsequently transitioned to E3 media.

Optogenetics—Single-cell-stage *Tg(y279*:*Gal4*; *UAS*:*Kaede)* embryos were co-injected with 25 pg of UAS:TagRFP-v2a-paGFP (kind gift from Harold Burgess lab), UAS:ChEF-v2a-mCherry,[64] or UAS:GtACR2-tdTomato plasmid[65] (Addgene plasmid #124236) and 25 pg of tol1 RNA. Individuals were raised in 200 μM PTU until 7dpf. At 7dpf, larvae were mounted in 2% low-melt agarose with the tail cut free and imaged using a Scientifica two-photon Vivoscope with Spectra-Physics MaiTai laser and 16x water immersion objective. Image acquisition was performed with ScanImage software through MATLAB. The laser was tuned to 940 nm (15 μW) and was focused on a single plane through the AMNs at 10x zoom. Each larva went through a stimulation series that consisted of 3 sequential recordings: 5 min of darkness followed by either a 20-s recording of dark (no laser), 940nm, and 1040nm stimulation, respectively. A μEye IDS1545LM-M CMOS camera recorded tail movement with a 12 mm lens, a long-pass 780 nm filter, and a short-pass 900 nm filter (Edmund Optics), and infrared illumination was provided using a Thorlabs fiber optic 850nm LED driver and fiber optic cable (M28L02). The camera's field of view was set to record the tail of each larva, and DAQtimer software was used to conduct real-time tracking of tail movement at 10 fps. Points were manually assigned to the tip of the tail for each recording frame as a measure of tail displacement from the original tail position.

Cell death analysis—To determine if the optogenetic stimulation resulted in cell damage, *Tg(y269*:*Gal4*; *UAS*:*mCherry)* embryos were raised in 200 μM PTU until 7dpf and mounted as described above. Control individuals were put through the optogenetic stimulation series. To induce photo-damage as a control, the 2-photon laser was tuned to 940nm (80 μW) and zoomed in 70x between the AMNs to focus laser power during a 10-s scan. Cell death was detected using acridine orange (AO) for 20 min (5 ng/μL in E3), followed by multiple washes in E3 for an hour. Finally, larvae were mounted in 2% low-melt agarose and imaged using a Thorlabs Confocal (TOPTICA iChrome CLE 50×lase, 10× objective).

QUANTIFICATION AND STATISTICAL ANALYSIS

Statistical analysis—Analysis was performed in MATLAB, RStudio, and Graphpad. Data in the figures and text represent means +− SEM. All t-tests were two-sided. Wilcoxon Signed Rank Sum tests were used for the match index compared to 0.5. Normality was determined using the Shapiro-Wilks test. ANOVAs were performed in Graphpad and Bonferroni corrected, or if normality test failed, Krustal Wallis test was used and corrected with the Dunn test. Chi-square statistics were performed in Graphpad. Chi-square analysis of neuron counts between enucleated and intact hemispheres was performed assuming equal number of responsive neurons per hemisphere and region based on a 50% value calculated from the total neuron count. Comparisons between control and PTZ neuron distrubutions were performed using the same critera, assuming equal numbers of responsiveness neurons per region and treatment.

Supplementary Material

Refer to Web version on PubMed Central for supplementary material.

ACKNOWLEDGMENTS

We want to thank Sarah Ackerman and Andrew Dacks for helpful comments on the manuscript. We thank Johnathan Huff for assistance with zebrafish care and preparation for CP assays. In addition, we thank Misha Ahrens, Harold Burgess, Steve Finkbeiner, and Jeremy Linsley for resources, including fish lines and plasmids. This work was supported by West Virginia University and Department of Biology startup funds, the Research and Scholarship Advancement award, Program to Stimulate Competitive Research funds, and NIGMS P20GM144230-02 (provided to E.J.H.).

REFERENCES

1. LeBlanc JJ, and Fagiolini M (2011). A “critical period” disorder? Neural Plast. 2011, e921680.
2. Paolicchi JM (2013). The timing of pediatric epilepsy syndromes: what are the developmental triggers? Ann. N. Y. Acad. Sci. 1304, 45–51. [PubMed: 24279892]
3. Takesian AE, and Hensch TK (2013). Balancing plasticity/stability across brain development. Prog. Brain Res. 207, 3–34. [PubMed: 24309249]
4. Wiesel TN, and Hubel DH (1963). SINGLE-CELL responses in striate cortex of kittens deprived OF VISION IN one eye. J. Neurophysiol. 26, 1003–1017. [PubMed: 14084161]
5. Wiesel TN, and Hubel DH (1965). Comparison of the effects of unilateral and bilateral eye closure on cortical unit responses in kittens. J. Neurophysiol. 28, 1029–1040. [PubMed: 5883730]
6. Nahmani M, and Turrigiano GG (2014). Deprivation-induced strengthening of presynaptic and postsynaptic inhibitory transmission in layer 4 of visual cortex during the critical period. J. Neurosci. 34, 2571–2582. [PubMed: 24523547]

7. Sun YJ, Espinosa JS, Hoseini MS, and Stryker MP (2019). Experience-dependent structural plasticity at pre- and postsynaptic sites of layer 2/3 cells in developing visual cortex. Proc. Natl. Acad. Sci. USA 116, 21812–21820. [PubMed: 31591211]
8. Kannan M, Gross GG, Arnold DB, and Higley MJ (2016). Visual deprivation during the critical period enhances layer 2/3 GABAergic inhibition in mouse V1. J. Neurosci. 36, 5914–5919. [PubMed: 27251614]
9. Chattopadhyaya B, Di Cristo G, Higashiyama H, Knott GW, Kuhlman SJ, Welker E, and Huang ZJ (2004). Experience and activity-dependent maturation of perisomatic GABAergic innervation in primary visual cortex during a postnatal critical period. J. Neurosci. 24, 9598–9611. [PubMed: 15509747]
10. Iwai Y, Fagiolini M, Obata K, and Hensch TK (2003). Rapid critical period induction by tonic inhibition in visual cortex. J. Neurosci. 23, 6695–6702. [PubMed: 12890762]
11. LeVay S, Wiesel TN, and Hubel DH (1980). The development of ocular dominance columns in normal and visually deprived monkeys. J. Comp. Neurol. 191, 1–51. [PubMed: 6772696]
12. Issa NP, Trachtenberg JT, Chapman B, Zahs KR, and Stryker MP (1999). The critical period for ocular dominance plasticity in the Ferret's visual cortex. J. Neurosci. 19, 6965–6978. [PubMed: 10436053]
13. Dräger UC (1978). Observations on monocular deprivation in mice. J. Neurophysiol. 41, 28–42. [PubMed: 621544]
14. Maffei L, Berardi N, Domenici L, Parisi V, and Pizzorusso T (1992). Nerve growth factor (NGF) prevents the shift in ocular dominance distribution of visual cortical neurons in monocularly deprived rats. J. Neurosci. 12, 4651–4662. [PubMed: 1334503]
15. Hensch TK, and Stryker MP (1996). Ocular dominance plasticity under metabotropic glutamate receptor blockade. Science 272, 554–557. [PubMed: 8614806]
16. Sipe GO, Petravicz J, Rikhye RV, Garcia R, Mellios N, and Sur M (2021). Astrocyte glutamate uptake coordinates experience-dependent, eye-specific refinement in developing visual cortex. Glia 69, 1723–1735. [PubMed: 33675674]
17. Khibnik LA, Cho KKA, and Bear MF (2010). Relative contribution of feedforward excitatory connections to expression of ocular dominance plasticity in layer 4 of visual cortex. Neuron 66, 493–500. [PubMed: 20510854]
18. Fagiolini M, Fritschy JM, Löw K, Möhler H, Rudolph U, and Hensch TK (2004). Specific GABAA circuits for visual cortical plasticity. Science 303, 1681–1683. [PubMed: 15017002]
19. Kameyama K, Sohya K, Ebina T, Fukuda A, Yanagawa Y, and Tsumoto T (2010). Difference in binocularity and ocular dominance plasticity between GABAergic and excitatory cortical neurons. J. Neurosci. 30, 1551–1559. [PubMed: 20107082]
20. Sommeijer J-P, Ahmadlou M, Saiepour MH, Seignette K, Min R, Heimel JA, and Levelt CN (2017). Thalamic inhibition regulates critical-period plasticity in visual cortex and thalamus. Nat. Neurosci. 20, 1715–1721. [PubMed: 29184199]
21. Jaepel J,Hübener M,Bonhoeffer T,andRose T(2017).Lateral geniculate neurons projecting to primary visual cortex show ocular dominance plasticity in adult mice. Nat. Neurosci. 20, 1708–1714. [PubMed: 29184207]
22. Krahe TE, and Guido W (2011). Homeostatic plasticity in the visual thalamus by monocular deprivation. J. Neurosci. 31, 6842–6849. [PubMed: 21543614]
23. Huh CYL, Abdelaal K, Salinas KJ, Gu D, Zeitoun J, Figueroa Velez DX, Peach JP, Fowlkes CC, and Gandhi SP (2020). Long-term monocular deprivation during juvenile critical period disrupts binocular integration in mouse visual thalamus. J. Neurosci. 40, 585–604. [PubMed: 31767678]
24. Hensch TK, Fagiolini M, Mataga N, Stryker MP, Baekkeskov S, and Kash SF (1998). Local GABA circuit control of experience-dependent plasticity in developing visual cortex. Science 282, 1504–1508. [PubMed: 9822384]
25. Horstick EJ, Bayleyen Y, Sinclair JL, and Burgess HA (2017). Search strategy is regulated by somatostatin signaling and deep brain photoreceptors in zebrafish. BMC Biol. 15, 4. [PubMed: 28122559]
26. Horstick EJ, Bayleyen Y, and Burgess HA (2020). Molecular and cellular determinants of motor asymmetry in zebrafish. Nat. Commun. 11, 1170. [PubMed: 32127541]

27. Hageter J, Waalkes M, Starkey J, Copeland H, Price H, Bays L, Showman C, Laverty S, Bergeron SA, and Horstick EJ (2021). Environmental and molecular modulation of motor individuality in larval zebrafish. Front. Behav. Neurosci. 15, 777778. [PubMed: 34938167]
28. Bell WJ, Cathy T, Roggero RJ, Kipp LR, and Tobin TR (1985). Sucrose-stimulated searching behaviour of Drosophila melanogaster in a uniform habitat: modulation by period of deprivation. Anim. Behav. 33, 436–448.
29. Gray JM, Hill JJ, and Bargmann CI (2005). A circuit for navigation in Caenorhabditis elegans. Proc. Natl. Acad. Sci. USA 102, 3184–3191. [PubMed: 15689400]
30. Hills TT, Kalff C, and Wiener JM (2013). Adaptive lévy processes and area-restricted search in human foraging. PLoS One 8, e60488. [PubMed: 23577118]
31. Bianco IH, Kampff AR, and Engert F (2011). Prey capture behavior evoked by simple visual stimuli in larval zebrafish. Front. Syst. Neurosci. 5, 101. [PubMed: 22203793]
32. Rombough P (2002). Gills are needed for ionoregulation before they are needed for O(2) uptake in developing zebrafish, Danio rerio. J. Exp. Biol. 205, 1787–1794. [PubMed: 12042337]
33. Miyares RL, de Rezende VB, and Farber SA (2014). Zebrafish yolk lipid processing: a tractable tool for the study of vertebrate lipid transport and metabolism. Dis. Model. Mech. 7, 915–927. [PubMed: 24812437]
34. Burrill JD, and Easter SS (1994). Development of the retinofugal projections in the embryonic and larval zebrafish (Brachydanio rerio). J. Comp. Neurol. 346, 583–600. [PubMed: 7983245]
35. Zhang RW, Wei HP, Xia YM, and Du JL (2010). Development of light response and GABAergic excitation-to-inhibition switch in zebrafish retinal ganglion cells. J. Physiol. 588, 2557–2569. [PubMed: 20498234]
36. Hooks BM, and Chen C (2007). Critical periods in the visual system: changing views for a model of experience-dependent plasticity. Neuron 56, 312–326. [PubMed: 17964248]
37. Hooks BM, and Chen C (2020). Circuitry underlying experience-dependent plasticity in the mouse visual system. Neuron 107, 986–987. [PubMed: 32910891]
38. Mueller T (2012). What is the thalamus in zebrafish? Front. Neurosci. 6, 64. [PubMed: 22586363]
39. Cheng R-K, Krishnan S, Lin Q, Kibat C, and Jesuthasan S (2017). Characterization of a thalamic nucleus mediating habenula responses to changes in ambient illumination. BMC Biol. 15, 104. [PubMed: 29100543]
40. Heap LAL, Vanwalleghem G, Thompson AW, Favre-Bulle IA, and Scott EK (2018). Luminance changes drive directional startle through a thalamic pathway. Neuron 99, 293–301.e4. [PubMed: 29983325]
41. Dunn TW, Mu Y, Narayan S, Randlett O, Naumann EA, Yang CT, Schier AF, Freeman J, Engert F, and Ahrens MB (2016). Brain-wide mapping of neural activity controlling zebrafish exploratory locomotion. Elife 5, e12741. [PubMed: 27003593]
42. Freeman J, Vladimirov N, Kawashima T, Mu Y, Sofroniew NJ, Bennett DV, Rosen J, Yang CT, Looger LL, and Ahrens MB (2014). Mapping brain activity at scale with cluster computing. Nat. Methods 11, 941–950. [PubMed: 25068736]
43. Kunst M, Laurell E, Mokayes N, Kramer A, Kubo F, Fernandes AM, Förster D, Dal Maschio M, and Baier H (2019). A cellular-resolution atlas of the larval zebrafish brain. Neuron 103, 21–38.e5. [PubMed: 31147152]
44. Rivlin-Etzion M, Zhou K, Wei W, Elstrott J, Nguyen PL, Barres BA, Huberman AD, and Feller MB (2011). Transgenic mice reveal unexpected diversity of on-off direction-selective retinal ganglion cell subtypes and brain structures involved in motion processing. J. Neurosci. 31, 8760–8769. [PubMed: 21677160]
45. Venugopalan V, Guerra A, Nahen K, and Vogel A (2002). Role of laser-induced plasma formation in pulsed cellular microsurgery and micromanipulation. Phys. Rev. Lett. 88, 078103. [PubMed: 11863944]
46. Smear MC, Tao HW, Staub W, Orger MB, Gosse NJ, Liu Y, Takahashi K, Poo MM, and Baier H (2007). Vesicular glutamate transport at a central synapse limits the acuity of visual perception in zebrafish. Neuron 53, 65–77. [PubMed: 17196531]

47. Marvin JS, Scholl B, Wilson DE, Podgorski K, Kazemipour A, Müller JA,Schoch S,Quiroz FJU,Rebola N,Bao H,et al. (2018). Stability, affinity, and chromatic variants of the glutamate sensor iGluSnFR. Nat. Methods 15, 936–939. [PubMed: 30377363]

48. Baier H, and Wullimann MF (2021). Anatomy and function of retinorecipient arborization fields in zebrafish. J. Comp. Neurol. 529, 3454–3476. [PubMed: 34180059]

49. Ackerman SD, Perez-Catalan NA, Freeman MR, and Doe CQ (2021). Astrocytes close a motor circuit critical period. Nature 592, 414–420. [PubMed: 33828296]

50. Huang RQ, Bell-Horner CL, Dibas MI, Covey DF, Drewe JA, and Dillon GH (2001). Pentylenetetrazole-induced inhibition of recombinant gamma-aminobutyric acid type A (GABA(A)) receptors: mechanism and site of action. J. Pharmacol. Exp. Ther. 298, 986–995. [PubMed: 11504794]

51. Baraban SC, Taylor MR, Castro PA, and Baier H (2005). Pentylenetetrazole induced changes in zebrafish behavior, neural activity and c-fos expression. Neuroscience 131, 759–768. [PubMed: 15730879]

52. Hortopan GA, Dinday MT, and Baraban SC (2010). Spontaneous seizures and altered gene expression in GABA signaling pathways in a mind bomb mutant zebrafish. J. Neurosci. 30, 13718–13728. [PubMed: 20943912]

53. Morgan JI, Cohen DR, Hempstead JL, and Curran T (1987). Mapping patterns of c-fos expression in the central nervous system after seizure. Science 237, 192–197. [PubMed: 3037702]

54. deCarvalho TN, Akitake CM, Thisse C, Thisse B, and Halpern ME (2013). Aversive cues fail to activate fos expression in the asymmetric olfactory-habenula pathway of zebrafish. Front. Neural Circuits 7, 98. [PubMed: 23734103]

55. Shainer I, Enrico K, Eva L, Mariam Al K, Nouwar M, Shachar S, Johannes L, Michael K, and Herwig B (2022). A single-cell resolution gene expression atlas of the larval zebrafish brain. Preprint at bioRxiv. 10.1101/2022.02.11.479024.

56. Schwarzkopf M, Mike CL, Samuel JS, Rachel I, Naeem H, Harry MTC, and Niles AP (2021). Hybridization chain reaction enables a unified approach to multiplexed, quantitative, high-resolution immunohistochemistry and in situ hybridization. Preprint at bioRxiv. 10.1101/2021.06.02.446311.

57. Johnston GAR (2014). Muscimol as an ionotropic GABA receptor agonist. Neurochem. Res. 39, 1942–1947. [PubMed: 24473816]

58. Rupprecht P, and Friedrich RW (2018). Precise synaptic balance in the zebrafish homolog of olfactory cortex. Neuron 100, 669–683.e5. [PubMed: 30318416]

59. Chandra D, Jia F, Liang J, Peng Z, Suryanarayanan A, Werner DF, Spigelman I, Houser CR, Olsen RW, Harrison NL, and Homanics GE (2006). GABAA receptor alpha 4 subunits mediate extrasynaptic inhibition in thalamus and dentate gyrus and the action of gaboxadol. Proc. Natl. Acad. Sci. USA 103, 15230–15235. [PubMed: 17005728]

60. Luo R, Partridge JG, and Vicini S (2013). Distinct roles of synaptic and extrasynaptic GABAAreceptors in striatal inhibition dynamics. Front. Neural Circuits 7, 186. [PubMed: 24324406]

61. Shao E, Scheetz SD, Xie W, and Burton EA (2018). Modulation of the zebrafish optokinetic reflex by pharmacologic agents targeting GABAA receptors. Neurosci. Lett. 671, 33–37. [PubMed: 29410359]

62. Rihel J, Prober DA, Arvanites A, Lam K, Zimmerman S, Jang S, Haggarty SJ, Kokel D, Rubin LL, Peterson RT, and Schier AF (2010). Zebrafish behavioral profiling links drugs to biological targets and rest/wake regulation. Science 327, 348–351. [PubMed: 20075256]

63. Reichert S, Pavón Arocas O, and Rihel J (2019). The neuropeptide galanin is required for homeostatic rebound sleep following increased neuronal activity. Neuron 104, 370–384.e5. [PubMed: 31537465]

64. Marquart GD, Tabor KM, Bergeron SA, Briggman KL, and Burgess HA (2019). Prepontine non-giant neurons drive flexible escape behavior in zebrafish. PLoS Biol. 17, e3000480. [PubMed: 31613896]

65. Antinucci P, Dumitrescu A, Deleuze C, Morley HJ, Leung K, Hagley T, Kubo F, Baier H, Bianco IH, and Wyart C (2020). A calibrated optogenetic toolbox of stable zebrafish opsin lines. Elife 9, e54937. [PubMed: 32216873]

66. Mueller T, Dong Z, Berberoglu MA, and Guo S (2011). The dorsal pallium in zebrafish, Danio rerio (Cyprinidae, Teleostei). Brain Res. 1381, 95–105. [PubMed: 21219890]

67. Avitan L, Pujic Z, Mölter J, Van De Poll M, Sun B, Teng H, Amor R, Scott EK, and Goodhill GJ (2017). Spontaneous activity in the zebrafish tectum reorganizes over development and is influenced by visual experience. Curr. Biol. 27, 2407–2419.e4. [PubMed: 28781054]

68. Pietri T, Romano SA, Pérez-Schuster V, Boulanger-Weill J, Candat V, and Sumbre G (2017). The emergence of the spatial structure of tectal spontaneous activity is independent of visual inputs. Cell Rep. 19, 939–948. [PubMed: 28467907]

69. Gambrill AC, Faulkner RL, and Cline HT (2018). Direct intertectal inputs are an integral component of the bilateral sensorimotor circuit for behavior in *Xenopus* tadpoles. J. Neurophysiol. 119, 1947–1961. [PubMed: 29442555]

70. Isa T, Marquez-Legorreta E, Grillner S, and Scott EK (2021). The tectum/superior colliculus as the vertebrate solution for spatial sensory integration and action. Curr. Biol. 31, R741–R762. [PubMed: 34102128]

71. Hoffmann KP, and Sherman SM (1974). Effects of early monocular deprivation on visual input to cat superior colliculus. J. Neurophysiol. 37, 1276–1286. [PubMed: 4436700]

72. Salay LD, and Huberman AD (2021). Divergent outputs of the ventral lateral geniculate nucleus mediate visually evoked defensive behaviors. Cell Rep. 37, 109792. [PubMed: 34610302]

73. Gordon JA, and Stryker MP (1996). Experience-dependent plasticity of binocular responses in the primary visual cortex of the mouse. J. Neurosci. 16, 3274–3286. [PubMed: 8627365]

74. Morgan JL, Berger DR, Wetzel AW, and Lichtman JW (2016). The fuzzy logic of network connectivity in mouse visual thalamus. Cell 165, 192–206. [PubMed: 27015312]

75. Karlstrom RO, Trowe T, Klostermann S, Baier H, Brand M, Crawford AD, Grunewald B, Haffter P, Hoffmann H, Meyer SU, et al. (1996). Zebrafish mutations affecting retinotectal axon pathfinding. Development 123, 427–438. [PubMed: 9007260]

76. Bridi MCD, de Pasquale R, Lantz CL, Gu Y, Borrell A, Choi SY, He K, Tran T, Hong SZ, Dykman A, et al. (2018). Two distinct mechanisms for experience-dependent homeostasis. Nat. Neurosci. 21, 843–850. [PubMed: 29760525]

77. Ranson A, Cheetham CEJ, Fox K, and Sengpiel F (2012). Homeostatic plasticity mechanisms are required for juvenile, but not adult, ocular dominance plasticity. Proc. Natl. Acad. Sci. USA 109, 1311–1316. [PubMed: 22232689]

78. Desai NS, Cudmore RH, Nelson SB, and Turrigiano GG (2002). Critical periods for experience-dependent synaptic scaling in visual cortex. Nat. Neurosci. 5, 783–789. [PubMed: 12080341]

79. Koyama M, Minale F, Shum J, Nishimura N, Schaffer CB, and Fetcho JR (2016). A circuit motif in the zebrafish hindbrain for a two alternative behavioral choice to turn left or right. Elife 5, e16808. [PubMed: 27502742]

80. Koyama M, Kinkhabwala A, Satou C, Higashijima S.i., and Fetcho J (2011). Mapping a sensory-motor network onto a structural and functional ground plan in the hindbrain. Proc. Natl. Acad. Sci. USA 108, 1170–1175. [PubMed: 21199937]

81. Severi KE, Böhm UL, and Wyart C (2018). Investigation of hindbrain activity during active locomotion reveals inhibitory neurons involved in sensorimotor processing. Sci. Rep. 8, 13615. [PubMed: 30206288]

82. Tropea D, Van Wart A, and Sur M (2009). Molecular mechanisms of experience-dependent plasticity in visual cortex. Philos. Trans. R. Soc. Lond. B Biol. Sci. 364, 341–355. [PubMed: 18977729]

83. Huang ZJ, Kirkwood A, Pizzorusso T, Porciatti V, Morales B, Bear MF, Maffei L, and Tonegawa S (1999). BDNF regulates the maturation of inhibition and the critical period of plasticity in mouse visual cortex. Cell 98, 739–755. [PubMed: 10499792]

84. Andreska T, Rauskolb S, Schukraft N, Lüningschrör P, Sasi M, Signoret-Genest J, Behringer M, Blum R, Sauer M, Tovote P, and Sendtner M (2020). Induction of BDNF expression in layer

II/III and layer V neurons of the motor cortex is essential for motor learning. J. Neurosci. 40, 6289–6308. [PubMed: 32651187]

85. Taha S, Hanover JL, Silva AJ, and Stryker MP (2002). Autophosphorylation of alphaCaMKII is required for ocular dominance plasticity. Neuron 36, 483–491. [PubMed: 12408850]
86. Putignano E, Lonetti G, Cancedda L, Ratto G, Costa M, Maffei L, and Pizzorusso T (2007). Developmental downregulation of histone posttranslational modifications regulates visual cortical plasticity. Neuron 53, 747–759. [PubMed: 17329213]
87. Liu C-H, Heynen AJ, Shuler MGH, and Bear MF (2008). Cannabinoid receptor blockade reveals parallel plasticity mechanisms in different layers of mouse visual cortex. Neuron 58, 340–345. [PubMed: 18466745]
88. Di Donato V, De Santis F, Auer TO, Testa N, Sánchez-Iranzo H, Mercader N, Concordet JP, and Del Bene F (2016). 2C-Cas9: a versatile tool for clonal analysis of gene function. Genome Res. 26, 681–692. [PubMed: 26957310]
89. Varshney GK, Pei W, LaFave MC, Idol J, Xu L, Gallardo V, Carrington B, Bishop K, Jones M, Li M, et al. (2015). High-throughput gene targeting and phenotyping in zebrafish using CRISPR/Cas9. Genome Res. 25, 1030–1042. [PubMed: 26048245]
90. Ghosh A, and Halpern ME (2016). Transcriptional regulation using the Q system in transgenic zebrafish. Methods Cell Biol. 135, 205–218. [PubMed: 27443927]
91. Bergeron SA, Hannan MC, Codore H, Fero K, Li GH, Moak Z, Yokogawa T, and Burgess HA (2012). Brain selective transgene expression in zebrafish using an NRSE derived motif. Front. Neural Circuits 6, 110. [PubMed: 23293587]
92. Buss RR, and Drapeau P (2001). Synaptic drive to motoneurons during fictive swimming in the developing zebrafish. J. Neurophysiol. 86, 197–210. [PubMed: 11431502]
93. Humphries DA, and Driver PM (1970). Protean defence by prey animals. Oecologia 5, 285–302. [PubMed: 28309783]
94. Simons AM (2011). Modes of response to environmental change and the elusive empirical evidence for bet hedging. Proc. Biol. Sci. 278, 1601–1609. [PubMed: 21411456]
95. Catania KC (2010). Born knowing: tentacled snakes innately predict future prey behavior. PLoS One 5, e10953. [PubMed: 20585384]
96. Ayroles JF, Buchanan SM, O'Leary C, Skutt-Kakaria K, Grenier JK, Clark AG, Hartl DL, and de Bivort BL (2015). Behavioral idiosyncrasy reveals genetic control of phenotypic variability. Proc. Natl. Acad. Sci. USA 112, 6706–6711. [PubMed: 25953335]
97. Buchanan SM, Kain JS, and de Bivort BL (2015). Neuronal control of locomotor handedness in Drosophila. Proc. Natl. Acad. Sci. USA 112, 6700–6705. [PubMed: 25953337]
98. Golia MT, Poggini S, Alboni S, Garofalo S, Ciano Albanese N, Viglione A, Ajmone-Cat MA, St-Pierre A, Brunello N, Limatola C, et al. (2019). Interplay between inflammation and neural plasticity: both immune activation and suppression impair LTP and BDNF expression. Brain Behav. Immun. 81, 484–494. [PubMed: 31279682]
99. Davison JM, Akitake CM, Goll MG, Rhee JM, Gosse N, Baier H, Halpern ME, Leach SD, and Parsons MJ (2007). Transactivation from Gal4-VP16 transgenic insertions for tissue-specific cell labeling and ablation in zebrafish. Dev. Biol. 304, 811–824. [PubMed: 17335798]
100. Tabor KM, Bergeron SA, Horstick EJ, Jordan DC, Aho V, Porkka-Heiskanen T, Haspel G, and Burgess HA (2014). Direct activation of the Mauthner cell by electric field pulses drives ultrarapid escape responses. J. Neurophysiol. 112, 834–844. 10.1152/jn.00228.2014. [PubMed: 24848468]
101. Scott EK, Mason L, Arrenberg AB, Ziv L, Gosse NJ, Xiao T, Chi NC, Asakawa K, Kawakami K, and Baier H (2007). Targeting neural circuitry in zebrafish using GAL4 enhancer trapping. Nat Methods 4, 323–326. 10.1038/nmeth1033. [PubMed: 17369834]
102. Tabor KM, Smith TS, Brown M, Bergeron SA, Briggman KL, and Burgess HA (2018). Presynaptic inhibition selectively gates auditory transmission to the brainstem startle circuit. Curr. Biol. 28, 2527–2535.e8. [PubMed: 30078569]
103. Schneider CA, Rasband WS, and Eliceiri KW (2012). NIH Image to ImageJ: 25 years of image analysis. Nat Methods 9, 671–675. 10.1038/nmeth.2089. [PubMed: 22930834]
104. RStudio: Integrated Development for R. (2020).

105. Pologruto TA, Sabatini BL, and Svoboda K (2003). ScanImage: flexible software for operating laser scanning microscopes. Biomed Eng Online 2, 13. [PubMed: 12801419]

106. Mu Y, Bennett DV, Rubinov M, Narayan S, Yang CT, Tanimoto M, Mensh BD, Looger LL, and Ahrens MB (2019). Glia accumulate evidence that actions are futile and suppress unsuccessful behavior. Cell 178, 27–43.e19. [PubMed: 31230713]

107. Tseng Q, Wang I, Duchemin-Pelletier E, Azioune A, Carpi N, Gao J, Filhol O, Piel M, Théry M, and Balland M (2011). A new micropatterning method of soft substrates reveals that different tumorigenic signals can promote or reduce cell contraction levels. Lab Chip 11, 2231–2240. [PubMed: 21523273]

Highlights

- Ocular dominance plasticity-like changes occur in larval zebrafish
- Asymmetric visual experience impacts behavior during a visual critical period
- Functional changes in the thalamus correlate with visual experience and behavior
- Inhibitory signaling is necessary for visually mediated changes in the thalamus

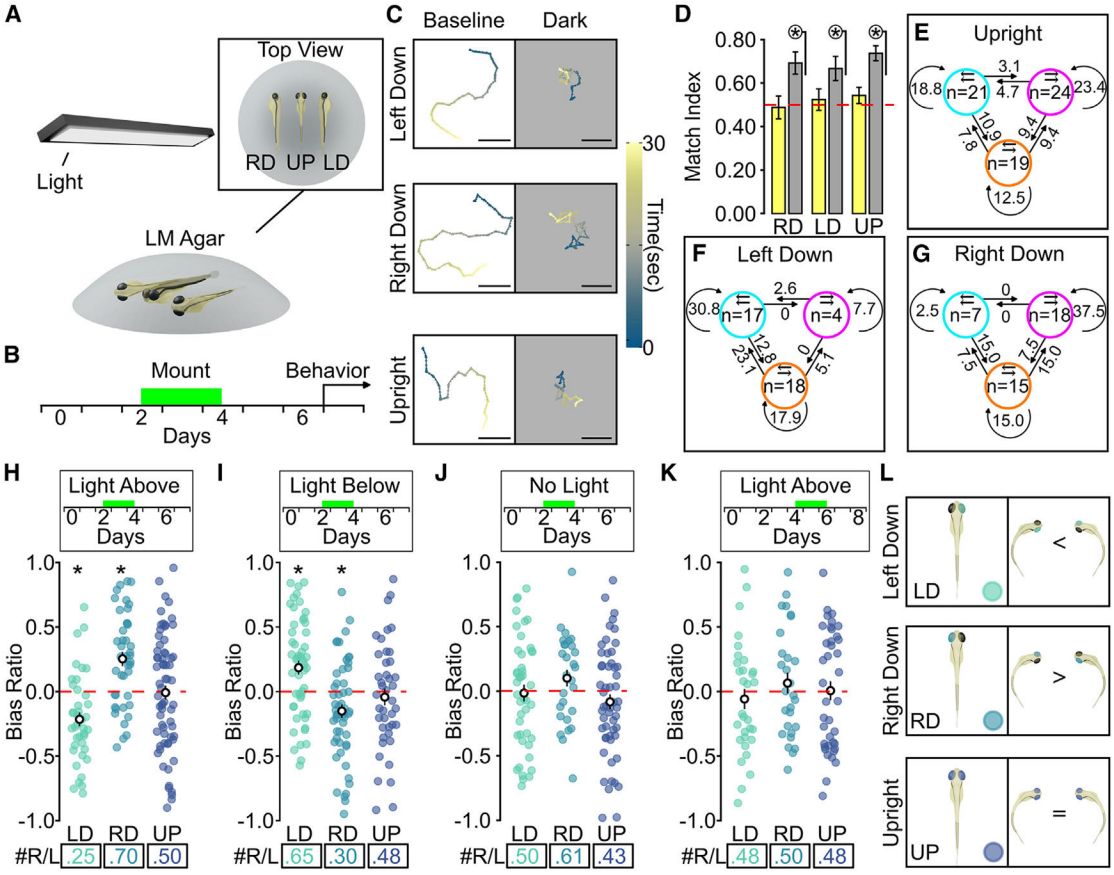

Figure 1. Asymmetric visual input directs larval zebrafish motor bias

(A) Diagram of the CP assay. The inset shows an overhead view of fish and mounting orientations (RD, right side down; UP, both eyes up; LD, left side down).

(B) Timeline of the CP assay for inducing turn bias direction. A green bar indicates the duration of embedding and visual control.

(C) Representative tracks of mounted individuals during baseline (left) and following loss of illumination (dark, right). Scale bars, 10 mm. The bar on the right shows time in seconds.

(D–G) Match index for mounted individuals during baseline (yellow) and dark (gray) recording conditions. A dotted red line indicates the random match index. A circled asterisk indicates $p < 0.05$, one-sample Wilcoxon signed rank test to 0.5 (RD, N = 40; LD, N = 35; UP, N = 62). Also shown are relative frequencies of paired directional transitions from the first two trials compared with the last two for (E) upright, (F) left-mounted, or (G) right-mounted fish. Numbers for the first two trials are denoted in colored circles for individuals that had repeated left (cyan), right (magenta), or random (orange) trials. Paired arrows in circles indicate turn direction over the first two trials. Arrows between circles indicate transition frequency, and adjacent numbers are percentages.

(H–K) Average BR (averaged over four trials per individual) for individuals in the CP. A box above each graph shows dpf (days), and the green bar indicates the time in the CP assay. Bottom: boxes show the ratio of right-biased (+BR) to left-biased (−BR) individuals per group. All CP assay BR graphs show these features. (H) CP assay from 2–4 dpf (LD, 39; RD, 40; UP, 62) with light overhead.

(I and J) Same as (H) with the light source rotated below the embedded larvae (I) (LD, N = 51; RD, N = 53; UP, N = 42) or with no photic experience (J) (LD, N = 44; RD, N = 28; UP, N = 54).

(K) CP assay performed later in development compared with (H)–(J). Behavior was tested at 8 dpf (LD, N, 31; RD, N = 28; UP, N = 39). *$p < 0.05$, one-tailed t test to 0. White circles with a black vertical line show the group mean and SEM.

(L) Diagram of visually mediated changes to turn bias direction during the CP. All error bars represent ±SEM.

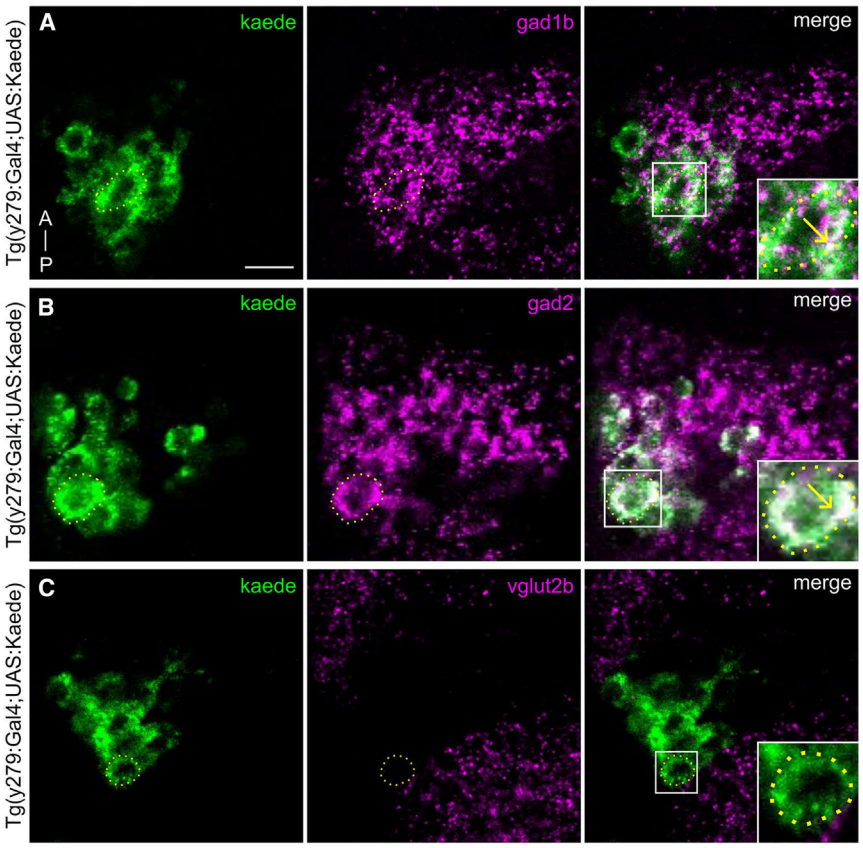

Figure 2. y279-specified AMNs are GABAergic

Fluorescence *in situ* hybridization (FISH) HCR of *Tg(y279:Gal4; UAS:kaede)* larvae at 3 dpf. All images are single-plane confocal scans showing AMNs from a single hemisphere. (A) Kaede mRNA (left, green), GAD1b mRNA (center, magenta), and merged (right). A dotted circle outlines a single cell body, and arrows indicate co-localization. Similar mRNA labeling was observed across fish: GAD2 (observed in 3 larvae)
(B) and VGlut2b (observed in 4 larvae).
(C) A similar pattern was observed in 3 larvae for each label.
Scale bar, 10 μm.

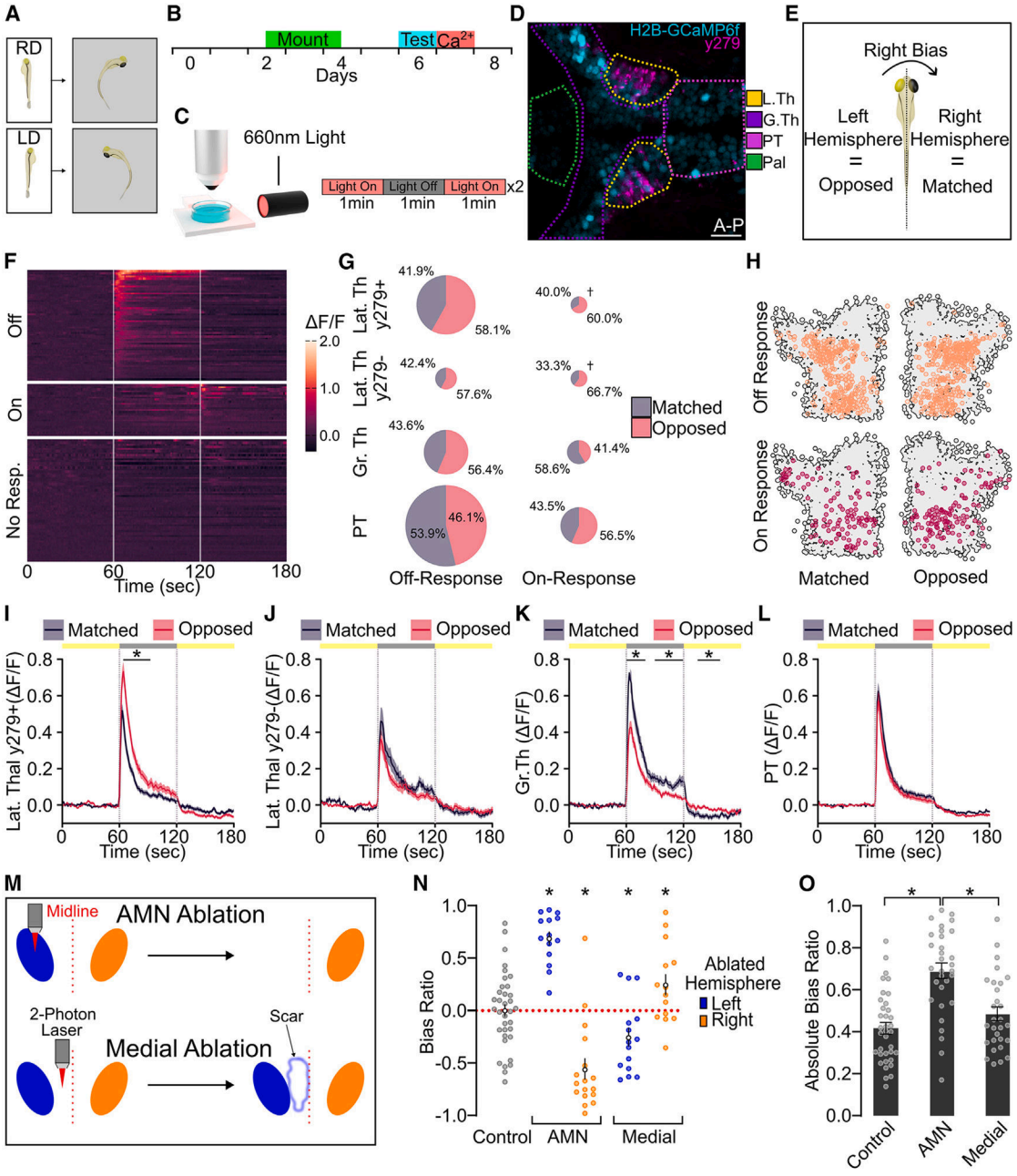

Figure 3. Thalamic neurons show functional asymmetries correlated to motor bias

(A–C) Outline of steps for calcium imaging experiments.

(A) Larvae were prepped in the CP assay prior to calcium imaging.

(B) Experiment outline showing the time period of the CP assay (mount, green), behavior testing to confirm turn bias (test, blue), and calcium imaging (Ca^{2+}, red).

(C) Schematic of calcium imaging set up on 2P and photo-stimulation series.

D) Representative segmentation of lateral thalamic (yellow), greater thalamic (purple), PT (pink), and pallium (green) neurons using *Tg(elavl3*: *H2B-GCaMP6f*; *y279 Gal4*; *UAS*: *nsfB-mCherry)*. Scale bar, 20μm.

(E) Example of matched and opposed hemispheres for a right-biased individual.

(F) Raster plot showing responses from a subset of lateral thalamus neurons. Vertical gray bars indicate light transition (0–60 s light ON, 6–120 s light OFF, 121–180 s light ON). Color scale, fluorescence change (ΔF/F).

(G) Proportions of matched and opposed visually evoked ON and OFF responses per region. Chart sizes are scaled to represent the proportion of neurons represented. A cross indicates groups with 50 or fewer neurons, which are set to a standard minimal scale.

(H and I) Spatial distribution for matched and opposed responses between hemispheres (OFF response, orange, N = 699; ON response, purple, N = 216). A gray outline indicates the position of neurons with no light response. OFF response mean and standard error for (I) lateral thalamic $y279^{+}$ (matched, N = 75; opposed, N = 104), (J) lateral thalamic $y279^{-}$ (matched, N = 28; opposed, N = 38), and

(K) greater thalamic (matched, N = 61; opposed, N = 79), and (L) PT regions (matched, N = 167; opposed N = 143). An asterisk with a bar indicates a two-tailed t test $p < 0.05$ for at least 10 consecutive time points.

(M) Diagram of unilateral 2P ablation.

(N) Average BR of larvae with left (blue) or right (orange) hemispheric ablation of AMNs (left, N = 14; right, N = 17), medial thalamic neurons (left, N = 15; right, N = 14), and unablated controls (gray, N = 36).

(O) Absolute BR of control (N = 36), AMN (N = 31), and medial thalamic neuron (N = 29) ablation. *$p < 0.05$ to 0. An asterisk with brackets indicates $p < 0.05$ between groups. All error bars and envelopes on line graphs represent ±SEM.

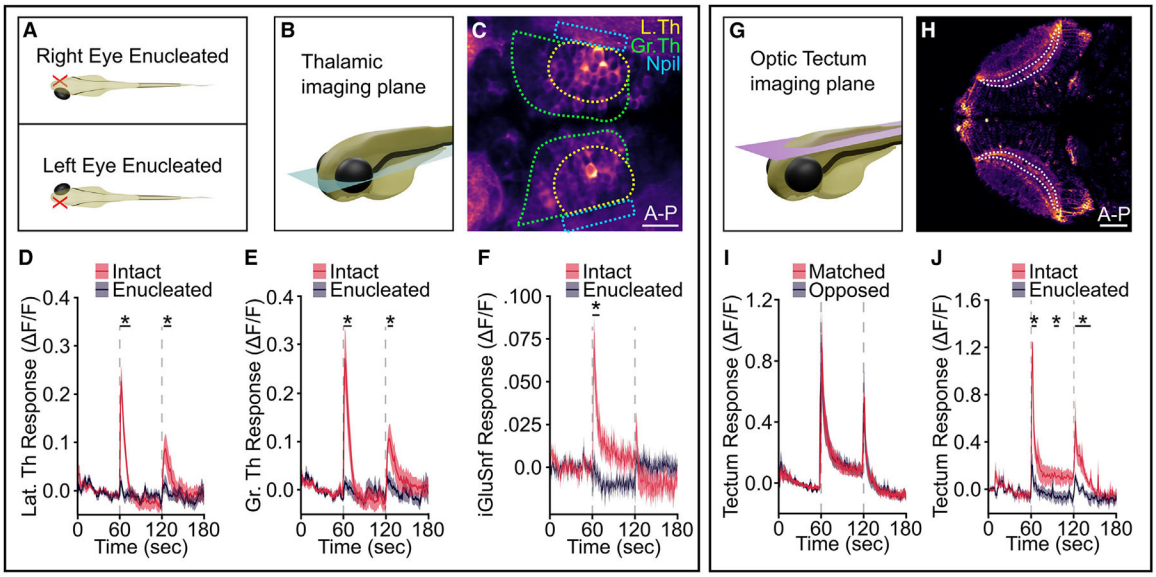

Figure 4. AMNs respond to visual input

(A) Schematic of unilateral enucleation.

(B) Representative image showing a single confocal plane for thalamic neuron imaging.

(C) Illustrative example showing regions for analysis in (D)–(F) (lateral thalamus [L. Th; white], greater thalamus [Gr. Th; green], and AMN neuropil [Npil; orange]). Scale bar, 20 μm. Shown are standardized calcium responses to visual stimuli in unilaterally enucleated larvae. Vertical dotted lines denote the time of light OFF (60 s) and light restoration (120 s). Solid lines are an average, and envelopes show ±SEM.

D) Calcium responses in the L. Th (N = 11) in the intact (red) and enucleated (purple) hemisphere.

(E) Same as (C), showing Gr. Th (N = 11) responses.

(F) iGluSnfer responses from intact (red) and enucleated (purple) hemispheres recorded from the adjacent AMN Npil (N = 9).

(G) Representative image showing a single confocal plane for optic tectum imaging.

(H) Illustrative region used for recording calcium responses in the optic tectum Npil. Scale bar, 50 μm.

(I) Npil responses for hemispheres matched to the direction of turn bias (red) or opposed (purple) (N = 13).

(J) Npil responses contralateral to the enucleated eye (red) or ipsilateral (purple) (N = 11). Asterisk and bar, two-tailed t test, $p < 0.05$ for at least three consecutive time points. Envelopes on line graphs represent ±SEM.

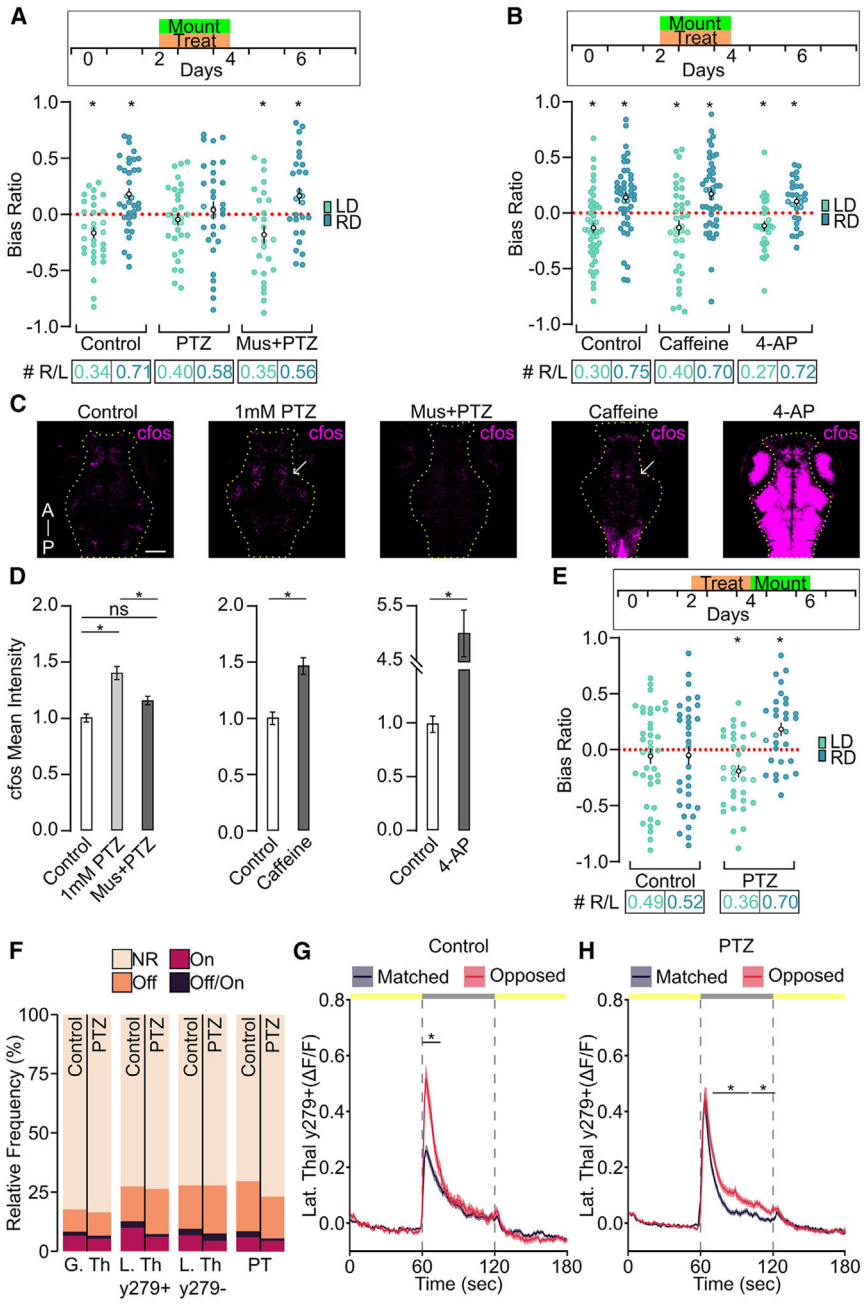

Figure 5. GABAergic signaling controls CP timing

(A) Average BR of larvae following asymmetric visual experience. A schematic (top box) shows the time in dpf (days) of CP assay mounting (green) and drug treatments (orange). Control (LD, N = 32; RD, N = 35), PTZ (LD, N = 30; RD, N = 31), and muscimol + PTZ (LD, N = 26; RD, N = 27). Bottom R/L values show the proportion of left BR (negative values) to right BR (positive value) individuals. A red line indicates random movement. (B) Same as in (A) with different activity-modulating drug treatments (control: LD, N = 46; RD, N = 47; 500 μM caffeine: LD, N = 37; RD, N = 43; 400 μM 4-AP: LD, N = 30; RD, N = 29).

(C) Representative c-fos mRNA labeling following drug treatments. Shown are single-plane confocal scans of 4-dpf larvae. An arrow indicates areas of increased c-fos expression. A yellow outline shows the area analyzed for c-fos signal quantification. Scale bar, 100 μM.
(D) Quantification of (C). Shown is the average mean intensity of c-fos from untreated controls (N = 41), PTZ (N = 16), muscimol + PTZ (N = 14), caffeine (N = 14), and 4-AP (N = 12). Values are standardized to the control.
(E) Same as in (A) with larvae prepped in the CP assay from 4–6 dpf (see timeline in the box above) (control: LD, N = 39; RD, N = 33; PTZ: LD, N = 33; RD, N = 30). *$p < 0.05$ to 0.0. An asterisk with lines in (D) shows $p < 0.05$ between groups.
(F–H) Frequency of photo-mediated responses for all regions in PTZ or control individuals (tan, no response [NR]; orange, OFF response; red, ON response; purple, OFF/ON response). Shown is the average OFF response for the matched (purple) or opposed (red) hemisphere based on positioning in the CP assay and expected turn bias direction for (G) control (matched, N = 123 neurons; opposed, N = 43 neurons from N = 19 larvae; N = 12 RD and N = 7 LD) and (H) PTZ-treated larvae (matched, N = 127 neurons; opposed, N = 110 neurons from N = 19 larvae; N = 12 RD and N = 7 LD). An asterisk with a bar indicates a two-tailed t test $p < 0.05$ for at least 10 consecutive time points comparing matched and opposed responses.
All error bars and envelopes on line graphs represent ±SEM.

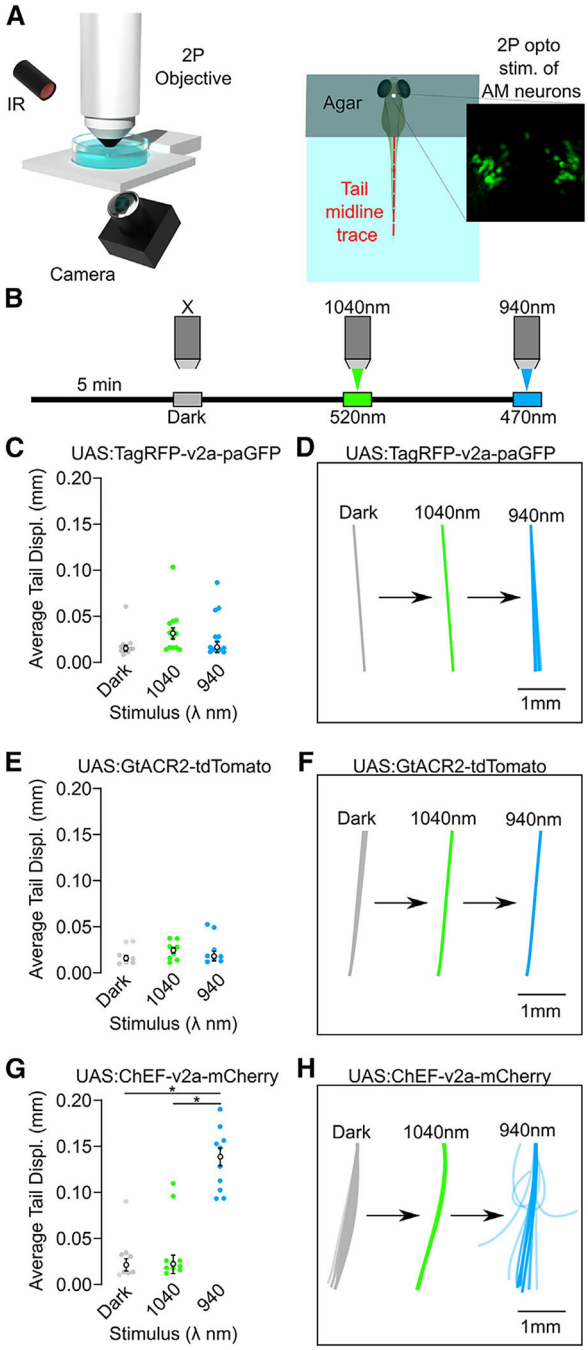

Figure 6. AMN activation drives motor responses

(A) Schematic of the 2P setup for optogenetic stimulation and tail recording (left) and a diagram of head-embedded larvae and field of view containing AMNs (right).

(B) Photic stimulation series and wavelengths.

(C) Average tail displacement (mm) of UAS:TagRFP-v2a-paGFP (control) larvae following no-stimulation dark controls (gray), 1,040-nm (green), and 940-nm laser (blue) exposure. Individuals tested, N = 13.

(D) Representative tail traces for analysis in (C) during dark control, 1,040-nm, and 940-nm recording.
(E and F) Optogenetic inhibition of AMNs using GtACR2, showing tail displacement (E) and illustrative tail trace examples (F) (N = 8).
(G and H) Same as above for UAS:ChEF-v2a-mCherry-injected individuals (N = 10). An asterisk with lines shows $p < 0.05$ between groups.
All error bars represent ±SEM.

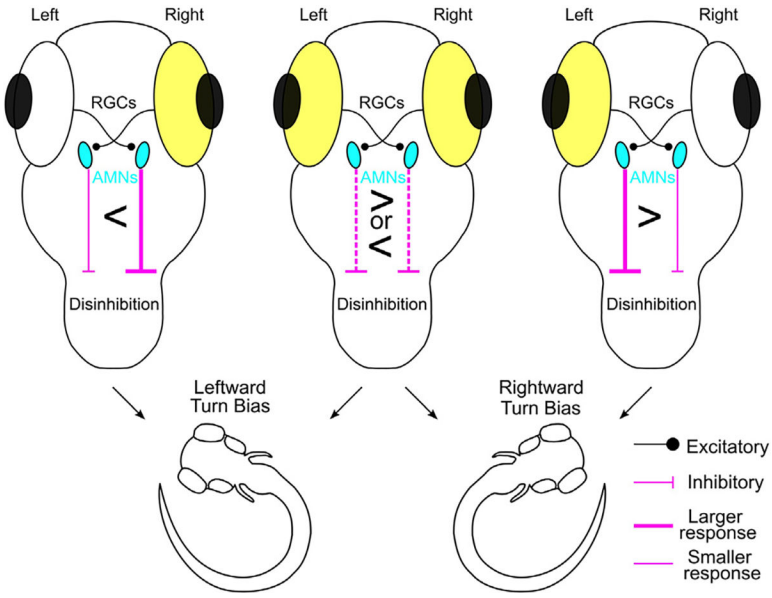

Figure 7. Circuit diagram

Shown is a representative diagram of the proposed circuit model and visual experience impact on turn bias. Excitatory connections are shown with circled ends and inhibitory connections with flat ends. Examples of visual plasticity are shown for right-eye, both eyes (center), and left-eye stimulation conditions. The stimulated eye is shown in yellow. Line thickness indicates response strength. We propose that asymmetric descending AMN disinhibitory signaling to premotor neurons releases motor activity to establish turn bias.

KEY RESOURCES TABLE

REAGENT or RESOURCE	SOURCE	IDENTIFIER
Chemicals, peptides, and recombinant proteins		
Phosphate buffered saline (PBS)	Gibco	70011–044
MS-222 (tricane methanesulfonate)	Syndel	200–226
Low-melting temperature agarose	Lonza	50084
1-phenyl 2-thiourea (PTU)	Sigma	P7629–10G
Pentylenetetrazole (PTZ)	Sigma	P6500–25G
Muscimol	Sigma	M1523–5MG
Caffeine	Sigma	BCCD7174
4-aminopyridine	Sigma	275875–1G
Gabaxadol hydrochloride	Sigma	T101–100MG
Tween 20	Sigma	P1379
Paraformaldehyde	Electron Microscopy Services	15710
Acridine Orange	Sigma	A6014
Experimental models: Organisms/strains		
TL Wildtype Zebrafish	ZIRC	ZL86
Tg(y279: Gal4)	Horstick et al., 2020[26]	ZDB-ALT-151216–33
Tg(UAS: Kaede)s1999t	Davison et al., 2007[99]	ZDB-ALT-070314–1
Tg(UAS: nsfb-mCherry)	Davison et al., 2007[99]	ZDB-TGCONSTRCT-070314–2
Tg(UAS: epNTR-tagRFPt)	Taboretal., 2014[100]	ZDB-TGCONSTRCT-141113–4
Tg(elavl3: GCaMP6f)	Freeman et al., 2014[42]	ZDB-TGCONSTRCT-150916–3
Tg(elavl3: H2B-GCaMP6f)	Dunn et al., 2016[41]	ZDB-TGCONSTRCT-150916–4
Et(hsp70l:Gal4-VP16)s1020tEt	Scott et al., 2007[101]	ZDB-ALT-070420–21
Oligonucleotides		
GAD1b	Molecular Instruments	NM_194419
GAD2	Molecular Instruments	NM_001017708
VGlut2b	Molecular Instruments	NM_001009982
kaede	Molecular Instruments	Stock probe mix
fosab/c-fos	Molecular Instruments	NM_205569
Recombinant DNA		
Plasmid: UAS: BGi-nls-GCaMP6s	Horstick et al., 2020[26]	NA
Plasmid: UAS: tagRFP-v2a-paGFP	Laboratory of Harold Burgess	NA
Plasmid: UAS: ChEF-v2a-mCherry	Marquart etl.al, 2019[64]	NA
Plasmid: UAS: GtACR2-tdTomato	Antinucci et al., 2020[65]	Addgene 124236
Plasmid: UAS: iGluSnfr.zf1	Taboretal., 2018[102]	Addgene108356
Deposited data		
Raw and analyzed data	Mendelay Data	https://doi.org/10.17632/bpj99zrshg.1

REAGENT or RESOURCE	SOURCE	IDENTIFIER
Software and algorithms		
Fiji/ImageJ	Schneider et al., 2012[103]	https://imagej.nih.gov/ij/
RStudio	RStudio Team, 2020[104]	https://cran.r-project.org/
GraphPad Prism	Graphpad	www.graphpad.com
MATLAB	MATLAB (R2021b)	https://se.mathworks.com/
ScanImage	Pologruto et al., 2003[105]	https://www.mbfbioscience.com/products/scanimage
mapzebrain	Kunstetal., 2019[43]	https://mapzebrain.org/home